Towards a pointing Model for GMRT antennas–Part III: Model parameters and implementation

by Subhashis Roy & Vasant Kulkarni

Internal Technical report

NCRA-TIFR
Pune-7

Table of contents

Towards a pointing model for GMRT antennas–Part III: Model parameters and implementation

February 23, 2009

Abstract

In this technical report, we have described a 7 parameter model which could reliably fit the observed azimuth and elevation pointing errors data from the GMRT antennas including refraction correction due to neutral atmosphere. The model parameters appear to remain stable for most of the antennas over time scale of about an year. This model is now applied in real time on regular basis, and we describe also the implementation of the model.

1 Introduction

Any mechanical structure built following a design do suffer from imperfections. For example, the azimuth axis of the GMRT antennas may not be truly vertical or the elevation axis not lying in the horizontal plane. Such errors would cause systematic difference between the apparent azimuth and elevation angles of the antennas and the true azimuth and elevation angle the antennas make resulting in pointing errors. Moreover, depending on the elevation angle, antenna could bend or its reflecting surface deviate from a true parabola due to changes in its support structure caused by gravitational bending. This also results in elevation dependent pointing error. Given that misalignment of axis is geometrical in nature, the resulting pointing errors could be corrected if the amount of misalignment for each antennas can be measured. If gravitational bending of support structures cause the effective axis of the antennas to shift by small amount, it also could be modelled. Hence, measuring pointing errors of the antennas are needed, and if found to be significant, there is need to model and apply corrections.

Need for such measurements was felt before, and strategies to measure pointing offsets accurately initiated. To measure pointing errors, antennas were used to scan a strong source ($\sim$ a few hundred Jy) with known angular speed and total power data for antennas recorded. However, this was possible only if a strong radio sources in the sky was visible (only a few of which are known), and one also needed to switch the automatic level controls (ALCs) off. Measurements of pointing errors were performed by fitting a Gaussian beam pattern to the observed total power as a function of time, which meant the speed of the scan and the start time of the scans was accurately known. However, occasionally at least one of the above (perhaps the start time) was not correct and the pointing errors appeared unreproducible for a few antennas when repeated. Also, the shape of the beam showed indications of saturation in some cases. Therefore, a new method, where a calibrator is observed using interferometric techniques at different known offsets from the pointing centre for all but the reference antennas in both azimuth and elevation has evolved. It is called the 'Grid-pointing', during which a calibrator is observed with 5-9 known offsets for $\sim$ 1 minute at each grid points in azimuth and elevation moving from one grid point to the next (separation of grid points are multiple of the grid size) and the maximum offset is within a factor of two of the FWHM of the antenna primary beam. One or two antennas are taken as reference, which just

tracks the source, and using cross-correlation data of the reference antenna with the rest of the antennas, their pointing errors are determined. This method is used to carry out all the pointing error measurements described here.

Previous measurements of pointing errors were typically carried out ["Towards a Pointing model for GMRT antennas–II" by Nimisha G Kanthria, Vasant Kulkarni & Rajaram Nityananda] by doing Grid-pointing on a single calibrator from rise to set. This was repeated on a few calibrators to cover a larger portion of the azimuth-elevation plane. It showed significant systematic variation of pointing error as a function of azimuth and elevation. They used the model of Greve et al. (1996, A&AS, 115, 379) to estimate the axis misalignment and gravitational bending parameters of the GMRT antennas. They found that (i) by using Greve et al. (1996) model, the residual rms pointing error of the antennas could be brought down to $\sim 1'$. They claimed the resultant model to satisfactorily correct the elevation pointing errors up to about 6 months, whereas the azimuth pointing errors could not be properly corrected beyond a couple of months.

Our Earth is covered with a layer of gaseous matter (atmosphere) and electromagnetic waves passing through such a layer bends due to refraction (except when the source is overhead) before reaching the antennas. Unless corrections are made for the bending of the waves, antennas when pointed to a source selected by their celestial position, the apparent position of the source will be different resulting in pointing error. However, no correction for atmospheric refraction has been incorporated while observing a source with the GMRT.

The present work was carried out to test if the measurements of pointing errors obtained are repeatable over longer time scales, to examine whether the model used by Greve et al. (1996) is really suited for the GMRT antennas, incorporate a refraction correction for the antenna positions and to apply corrections for the Pointing errors in real time during observations.

2 Observations and data reductions:

To measure the pointing errors for the GMRT antennas, several observations during test times were carried out for durations $\gtrsim$ 8 hours. Some of these observations were intended to find antenna based jumps in pointing errors at certain hour angles. However, here we will mostly describe observations which were specifically used to measure and model the pointing errors of the antennas. Observations were carried out on $26^{\rm th}$ to $27^{\rm th}$ December 2007 for a total of ~ 36 hours. In the first 12 hours of the observing time, 3 calibrator sources seen South from our latitude, 0745+101, $0744-064$ and $0837-198$ were observed in multiple snapshots mode using Grid-pointing from rise to set. In the next 12 hours, another 3 northern latitude sources 1927+739, 1924+334, and 1400+621 or 2148+611 were observed in the same manner, which resulted in a good coverage of the azimuth (AZ) − elevation (EL) plane (total 52 pointing error measurements at different AZ and EL) (Fig. 1). During the last 12 hours, the 3 calibrators observed during the first 12 hours were re-observed to check if the pointing errors could be reproduced for the earlier AZ and EL positions.

Seven grid points were used for each set of AZ and EL Grid-pointing and the grid size was $6'$. W01 and S02 were used as reference antennas and the observing frequency was chosen to be 1280 MHz, so that the primary beam sizes remain small thereby improving the accuracy of the pointing error measurements.

We used the programme 'pxget' (as developed by Vasant Kulkarni) to measure AZ and EL pointing errors from the Grid-pointing observations.

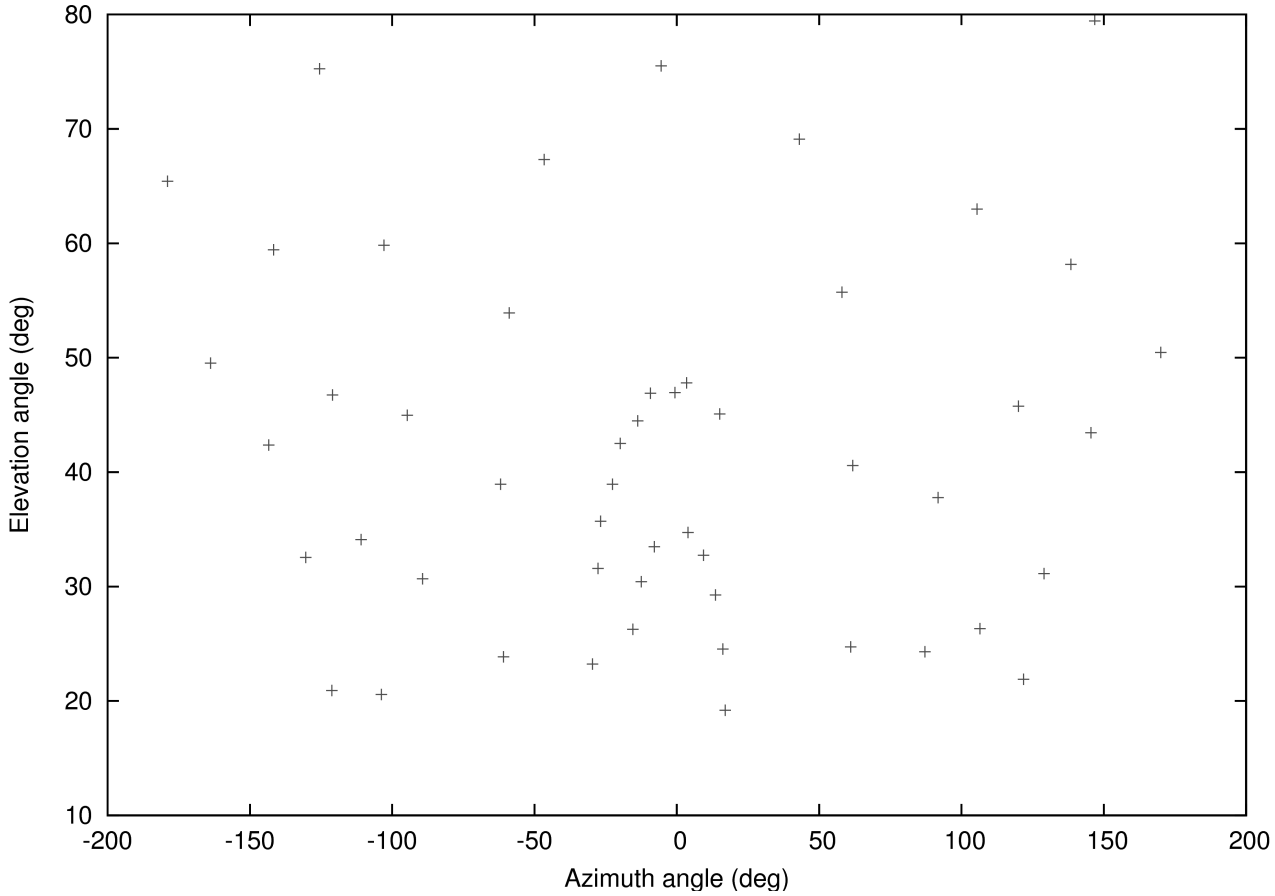

Figure 1. Mean azimuth and elevation angles of calibrator source during each set of Grid-pointing observations on 26-27 Dec 2007.

3 Results & Discussions:

Measured pointing errors as a function of hour angle with several antennas are shown in Fig. 2, which shows systematic variation of pointing errors as a function of Hour angle. For comparison, we also used the programme 'plotnew' (developed by Vasant Kulkarni), which produced the plot shown in Fig. 3. While producing the plot, the pointing errors were fitted to the model of Greve et al. (1996) and the fitted values subtracted. Rms errors before the fitting have been indicated in the plots by RMSB, and after subtracting the fit by RMSA. Among the antennas shown, except one (S04) (note that S02 was used as a reference antenna, for which errors are not determined), the RMSA reduces by ~ 2 and the systematics are reduced to a large extent. The scatter of the residual pointing errors is of $\sim 1'$, which is in accordance with the designed pointing accuracy of the GMRT antennas. The pointing offset of the antenna S04 is found to show occasional sudden changes in its pointing error (*jumps*) and is likely to be its hardware related, and could not be modelled properly.

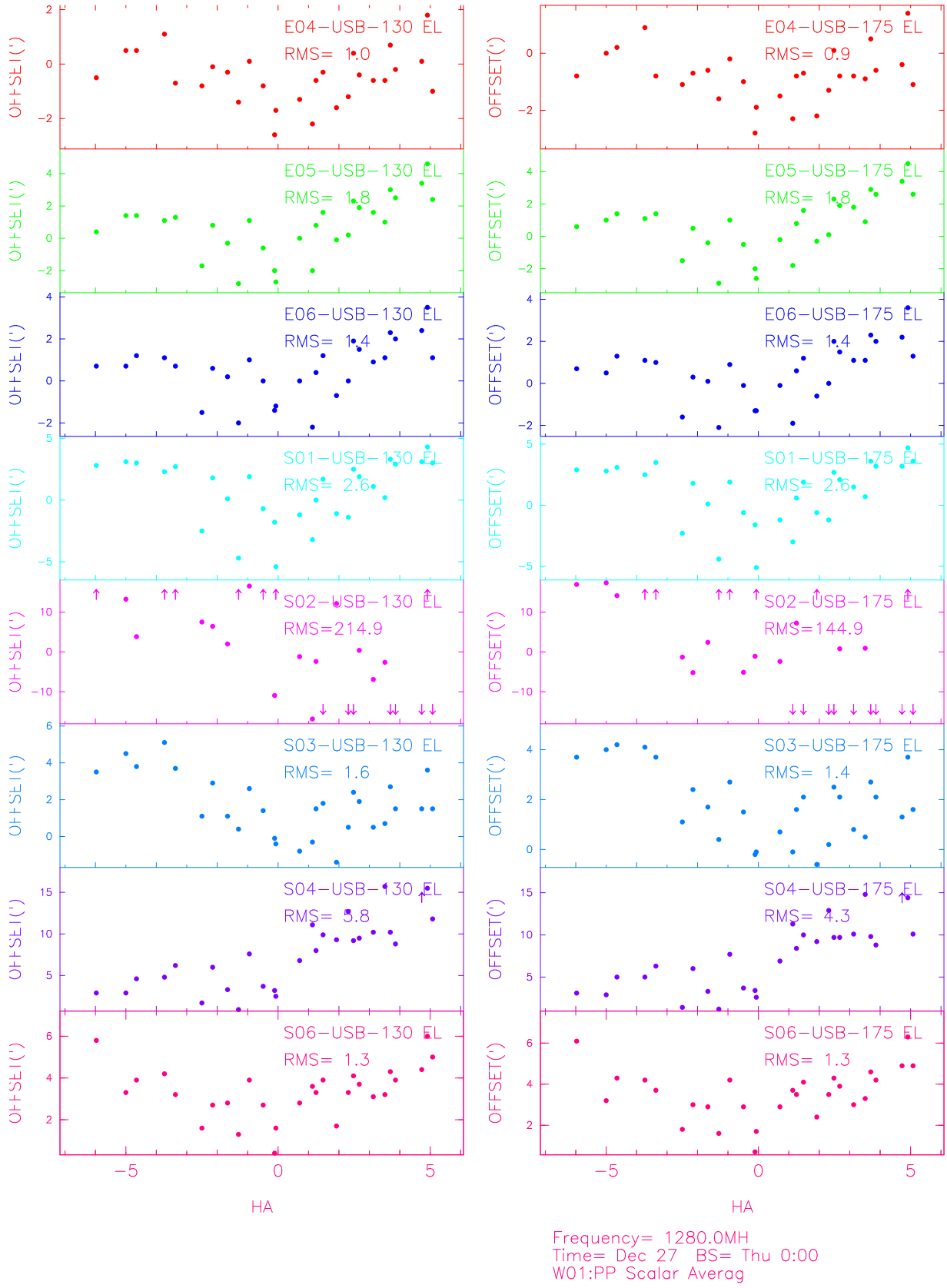

Figure 2. Measured pointing errors for several antennas as a function of Hour angle.

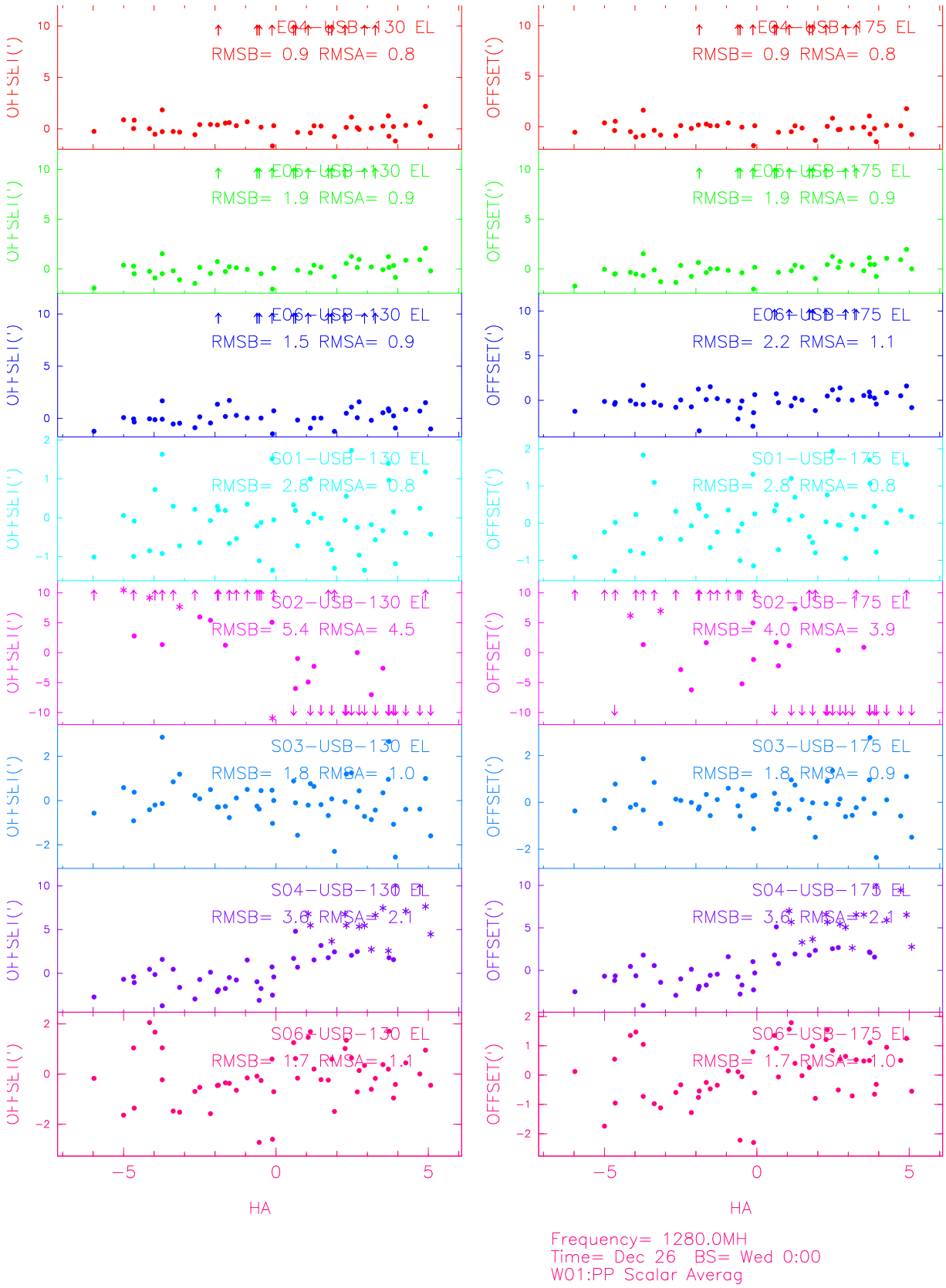

Figure 3. Pointing errors for several antennas after subtracting the model fit of Greve et al. (1996).

3.1 Testing the existing pointing model

The model of Greve et al. (1996) consider several causes of pointing errors during mechanical movements of the antennas along AZ and EL and its components in the sky plane in horizontal and vertical directions are given in Table 1.

Table 1. Pointing parameters P_i

Type of error		$H_i(A, E)$	$V_i(A, E)$
Zero–offset Az–encoder	P_1	$\cos E$	0
Collimation error [a]	P_2	1	0
Inclination El–axis [b]	P_3	$\sin E$	0
Inclination Az–axis [c] N – S	P_4	$\cos A \sin E$	$-\sin A$
Inclination Az–axis [c] E – W	P_5	$\sin A \sin E$	$\cos A$
Zero–offset El–encoder	P_6	0	1
Gravitational bending [d]	P_7	0	$\cos E$
Gravitational bending [d]	P_8	0	$\sin E$

[a] non–orthogonality of the radio beam axis and the elevation axis, also non–colinearity of the radio beam axis and the azimuth axis for zenith direction of the telescope [note that the best–fit geometrical reflector axis still may fulfill this orthogonality/ colinearity condition].

[b] non–orthogonality of azimuth and elevation axis.

[c] the values $\delta h_A = \delta h_4 + \delta h_5$ and $\delta v_A = \delta v_4 + \delta v_5$ determine the inclination of the azimuth axis.

[d] the values $\delta h_B = \delta h_8 + \delta h_9$ and $\delta v_B = \delta v_8 + \delta v_9$ determine the bending (gravitational deformation) of the telescope.

If their model is suitable for GMRT antennas, then the inclination of azimuth axis in the N-S and E-W direction (P4 and P5 in Table 1) as determined from the horizontal and vertical displacements of the antennas will match within the measurement errors. Fig. 4 shows a plot of P4 as determined from pointing errors along AZ (Green) and EL (Red) directions for all the antennas. However, as can be seen from the plot (Fig. 4), the values of P4 for most of the antennas as determined from the EL data appear to be higher than values derived from the AZ data.

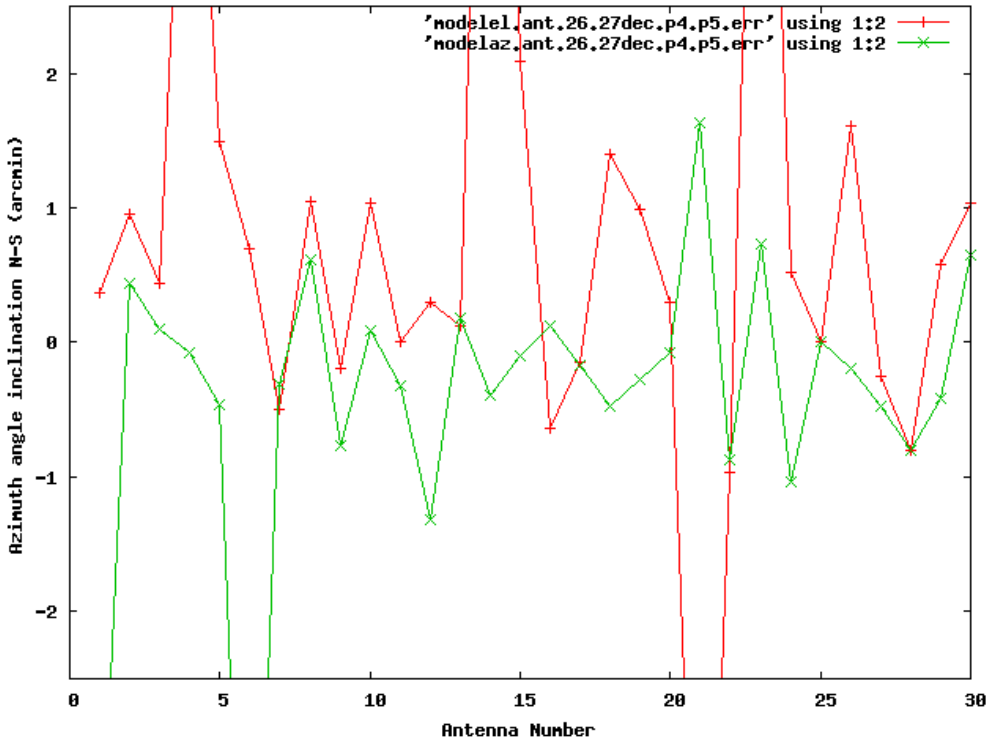

Figure 4. Inclination of AZ axis (N-S) (P4) as determined from AZ (Green) and EL (Red) pointing error data for all the 30 antennas.

From the fit of the model of Greve et al. (1996) to the EL pointing error data which are reliable, we have also tabulated the Zero-offset of the EL encoders (P6) and the gravitation terms (P7 & P8) and their errors in Table 2. From the table it is found that for most of the antennas the measurement errors on each of these terms are significantly higher than expected (predicts much higher errors in the overall fit for any AZ and EL values when errors in each parameters are assumed independent) from the overall error in fitting, which has to be $\sim 1'$ to get an overall rms error of $\sim 1'$ after subtracting the fit from the actual pointing error measurements (Fig. 3).

Table 2

Ant. name	P6	Err. on P6	P7	Err. on P7	P8	Err. on P8
C00	-3.70	2.67	3.83	1.93	4.11	2.01
C01	-4.94	2.45	10.3	1.77	-2.68	1.84
C02						
C03						
C04	-0.48	2.31	5.10	1.67	-1.92	1.74
C05						
C06	-0.75	2.41	2.67	1.73	0.69	1.81
C08	-0.71	2.10	4.37	1.51	-0.64	1.58
C09	3.375	2.56	-1.9	1.84	-8.62	1.92
C10	1.647	2.28	2.37	1.65	-2.06	1.72
C11	11.98	2.52	-3.3	1.82	-11.7	1.90
C12	4.717	1.98	1.24	1.43	-4.96	1.49
C13	10.84	2.12	-4.1	1.53	-10.4	1.59
C14						
E02						
E03	-2.27	2.55	3.43	1.84	-2.90	1.92
E04	-2.57	4.06	2.30	3.05	-0.35	2.91
E05	-0.70	4.27	4.01	3.21	-3.72	3.06
E06	-0.29	3.42	2.53	2.52	-3.48	2.55
S01	-2.67	2.21	8.29	1.59	-5.10	1.66
S02						
S03	6.751	2.41	-1.0	1.74	-7.61	1.81
S04	0.592	3.40	6.97	2.43	1.31	2.58
S06	12.26	2.39	-3.9	1.72	-10.4	1.79
W01						
W02	3.215	2.49	5.80	1.79	-8.24	1.87
W03	2.490	2.24	-1.6	1.61	-3.83	1.69
W04	5.066	2.08	-1.1	1.50	-5.45	1.56
W05	4.757	2.41	2.05	1.73	-4.57	1.82
W06	2.861	4.63	2.28	3.47	-6.05	3.31

Lack of consistency of inclination of AZ axis as determined from AZ and EL data (e.g. P4), and errors on fitted parameters being higher than the residuals after the fit indicates that the model used was not appropriate for the data. If the number of free parameters in a model is more than what is required to fit a data set, the measured parameters and their errors won't be independent. This is likely to be the case described above, and therefore a visualisation of the data is needed to identify the systematic patterns in the data, which could lead to an appropriate model, and is described in Sect. 3.2.

3.2 Finding new model parameters:

3.2.1 Pointing error due to refraction from the atmosphere:

Earth's atmosphere introduces refraction for any electromagnetic waves passing through it. Assuming the Earth as a sphere, and its neutral atmosphere to have a thickness much smaller compared to its radius, it is found that for elevation angle not too small ($>$ a few degrees), $\Delta\mathrm{EL} = 0.933.\cot(\mathrm{EL}) - 0.0012.\{\cot(\mathrm{EL})\}^3$, (COESA, US Standard Atmosphere, 1976, NOAA-S/T 76-1562, US Govt. Printing Office, Washington, DC (COESA 1976)) where ΔEL is the apparent change in the EL angle of an object in the sky. This leads to a $\Delta\mathrm{EL} = 3'$ for an object with EL=17° (lower limit of EL angle for GMRT) which is significant. Since neglecting the 2nd term in the above expression leads to an error of $\lesssim 0.04'$ in the refraction correction, we use only the 1st term in the expression in the rest of this report, and while implementing the above for pointing correction at GMRT. It should be noted that the shortcomings of the model of Greve et al. (1996) to describe the pointing error data of the GMRT as described above do not go away after correcting for the pointing error due to refraction from the neutral atmosphere.

3.2.2 Visualisation of pointing errors and deriving new model parameters

Since pointing error is expected to depend on the direction of the antennas, which is described by its AZ and EL, we visualised the pointing errors as a function of AZ and EL from 3-D graphs as produced by 'gnuplot'. After examining them, we find certain systematic patterns, and as a representative case it is shown for the antenna C01, for which the systematic effects are quite pronounced. Fig. 5 shows the Pointing errors after subtracting the contribution of Refraction with EL along the x-axis. A steady increase of the errors with decrease of EL is observed while it appear to saturate near EL=30°. This is likely to be due to gravitational bending of the structure and consequent shift of the focal point of the antennas. The errors appear to follow a *cos*(EL) pattern in the sky, and after fitting such a term (d.*cos*(EL), where 'd' is a constant), the residuals are shown in Fig. 6. To check any AZ dependency of the residuals, we plot the same with the AZ direction shown along x-axis (Fig. 7). A quasi sinusoidal pattern is seen along AZ, and we fitted a function 'f.*cos*(AZ-g)' to it, where 'f' and 'g' are are constants. After subtracting this fit, the residuals are shown in Fig. 8. Though subtracting the fit did not reduce the scatter drastically, except a few outliers, the spread of the data from Zero error did go down after subtraction.

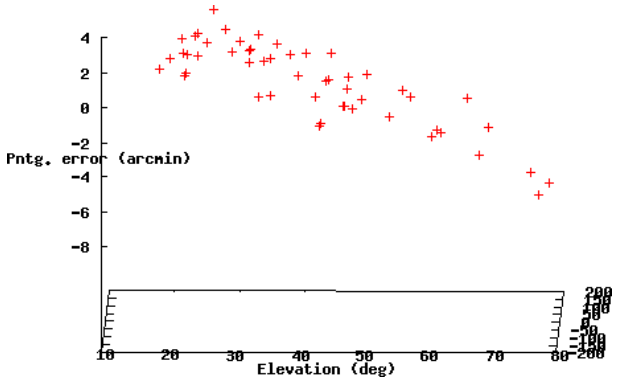

Figure 5. A 3-d plot of the 'EL pointing error -refraction' for the antenna C01 with EL along x-axis.

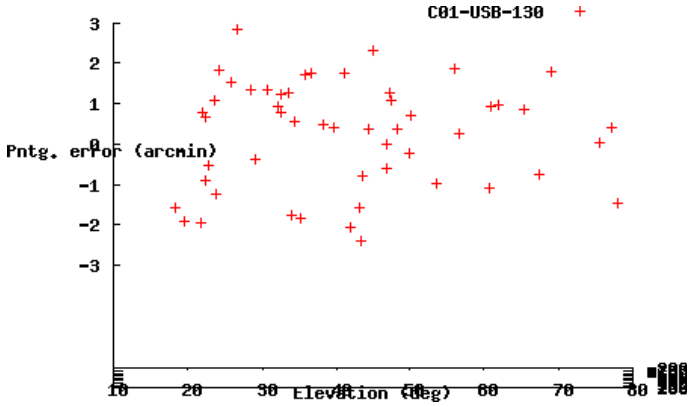

Figure 6. Same as above except the plot shows 'EL pointing error -refraction -d.*cos*(EL) -e'.

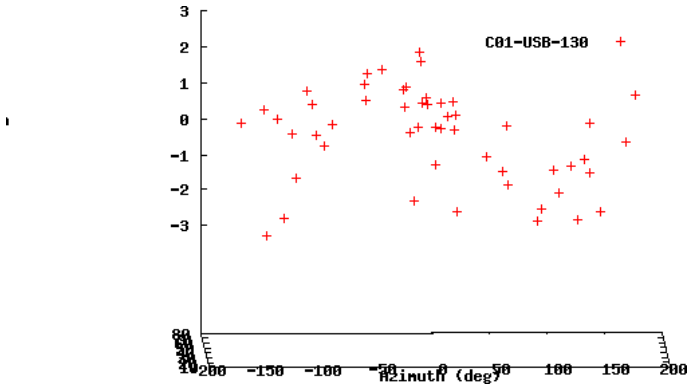

Figure 7. Same as above but the plot is rotated to show AZ along x-axis.

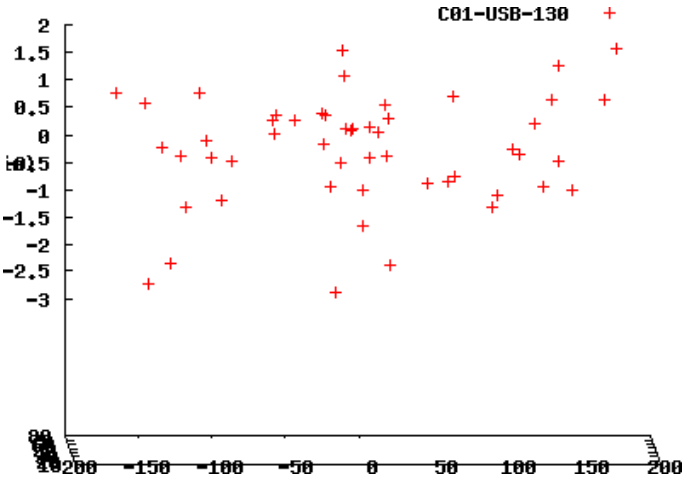

Figure 8. Plot of 'EL pointing error -refraction -d.*cos*(EL) -e -f.*cos*(AZ -g)' with AZ along x-axis (d, e, f, g are constants measured from the fit).

Similar efforts have also been made for AZ pointing errors. Fig. 9 shows AZ pointing errors with EL along x-axis. This pattern appears similar (except an offset) to what was observed in Fig. 5 and we fitted a function 'a.cos(EL) − b' to the data, and the residuals are shown in Fig. 10, which shows large reduction in systematics. Plotting the same with AZ along x-axis (Fig. 11) shows quasi-sinusoidal pattern at low level. Therefore, we have fitted a function 'c.cos(AZ)' and after subtracting the fit, the residuals are shown in Fig. 12, which shows reduction in AZ errors to $\sim 1'$ level.

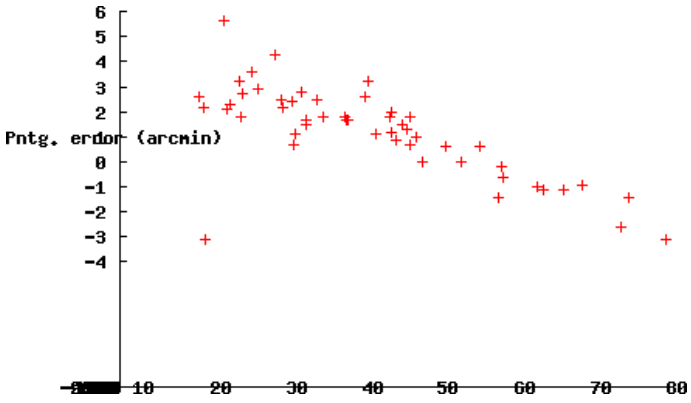

Figure 9. A 3-d plot of the AZ pointing error with EL along x-axis.

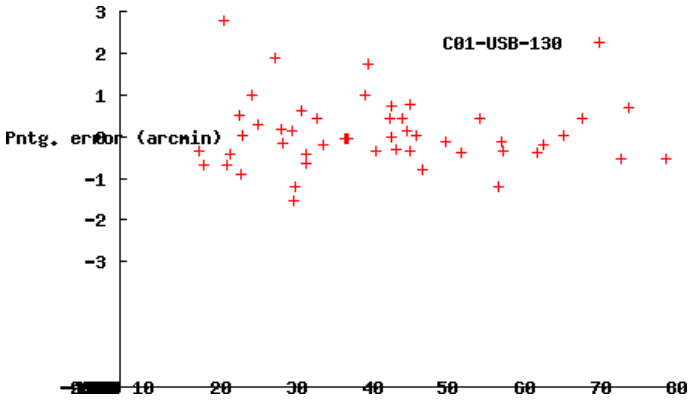

Figure 10. Same as above except that 'AZ pointing error -c.cos(EL) -b' is plotted.

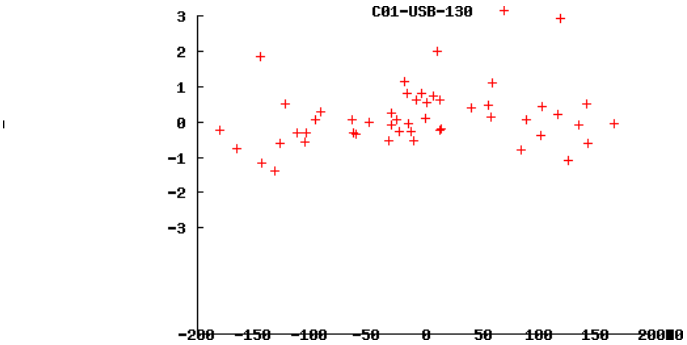

Figure 11. Same as above, but AZ is indicated along x-axis.

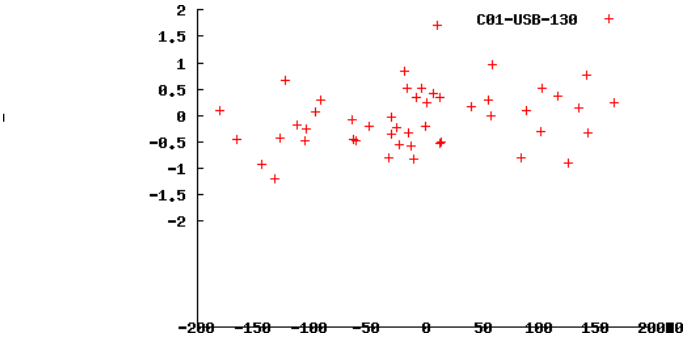

Figure 12. A plot of 'AZ pointing error − c.cos(EL) − b − a.cos(AZ)' with AZ along x-axis (a, b, c are constants determined from the fit).

We have provided all the reliable fit parameters to all the antennas in Table 3. The rightmost column indicates the reduced-χ^2 with an assumed rms error of $1'$. For most of the antennas, a reduced-χ^2 ~ 1 indicates validity of the fit. We also note that the errors on each of the fitted parameters are significantly less than scatter of the residuals after subtracting the fit, indicating independence of the fitted parameters.

We note that according to the new model, AZ and EL pointing errors (ΔAZ & ΔEL) are described by:

ΔAZ=a.cos(AZ)+b+c.cos(EL) ->(1)

ΔEL=0.933.cot(EL)+d.cos(EL)+e+f.cos(AZ-g), ->(2)

where a, b, c, d, e and f are constants to be determined from fit, and AZ and EL are measured in degrees.

Table 3

	a (′)	b (′)	c (′)	Chi−square	d (′)	e(′)	f (′)	g (degrees)	Chi−square
C00	−2.66 +/− 0.22	−0.54 +/− 0.54	7.13 +/− 0.78	0.95	−3.0 +/− 1.0	2.55 +/− 0.7	1.1 +/− 0.2	−19.8 +/− 15.2	1.94
C00	−2.74 +/− 0.22	−0.64 +/− 0.54	7.39 +/− 0.77	0.93	−2.8 +/− 0.8	2.56 +/− 0.6	1.0 +/− 0.2	−32.1 +/− 12.8	1.33
C01	0.403 +/− 0.22	−3.65 +/− 0.60	6.67 +/− 0.83	1.26	9.57 +/− 0.7	−7.3 +/− 0.5	1.1 +/− 0.2	−48.7 +/− 10.4	1.02
C01	0.330 +/− 0.22	−3.81 +/− 0.59	6.83 +/− 0.81	1.22	9.91 +/− 0.7	−7.6 +/− 0.5	1.2 +/− 0.2	−63.8 +/− 9.05	0.93
C02									
C02									
C03									
C03									
C04	−0.34 +/− 0.12	−3.59 +/− 0.33	7.44 +/− 0.46	0.39	4.08 +/− 0.6	−1.9 +/− 0.4	−1. +/− 0.1	80.77 +/− 6.29	0.71
C04	−0.33 +/− 0.14	−3.58 +/− 0.39	7.80 +/− 0.53	0.52	3.56 +/− 0.5	−2.1 +/− 0.4	−1. +/− 0.1	81.43 +/− 5.77	0.66
C05									
C05									
C06	−0.17 +/− 0.20	0.738 +/− 0.55	−0.3 +/− 0.76	1.06	−0.8 +/− 0.7	0.97 +/− 0.5	0.7 +/− 0.1	41.97 +/− 15.3	0.92
C06	−0.10 +/− 0.20	0.569 +/− 0.56	0.11 +/− 0.77	1.10	−1.0 +/− 0.7	1.19 +/− 0.5	0.7 +/− 0.2	28.58 +/− 16.8	1.11
C08	0.631 +/− 0.15	1.499 +/− 0.41	1.06 +/− 0.56	0.58	1.70 +/− 0.6	−0.5 +/− 0.4	1.1 +/− 0.1	−64.6 +/− 8.42	0.67
C08	0.565 +/− 0.15	1.323 +/− 0.41	1.08 +/− 0.57	0.60	2.17 +/− 0.5	−0.6 +/− 0.3	1.2 +/− 0.1	−71.7 +/− 6.34	0.48
C09	−0.41 +/− 0.22	−7.46 +/− 0.59	10.8 +/− 0.82	1.23	2.74 +/− 0.8	−6.8 +/− 0.6	−0.4 +/− 0.2	−140. +/− 28.1	1.26
C09	−0.56 +/− 0.18	−7.18 +/− 0.48	10.5 +/− 0.66	0.79	3.07 +/− 0.7	−6.9 +/− 0.5	−0.3 +/− 0.2	−156. +/− 33.8	0.95
C10	0.096 +/− 0.14	1.297 +/− 0.38	−0.3 +/− 0.53	0.52	1.24 +/− 0.6	−0.0 +/− 0.5	0.9 +/− 0.2	−109. +/− 10.7	0.87
C10	0.168 +/− 0.15	1.564 +/− 0.42	−0.9 +/− 0.58	0.62	1.20 +/− 0.5	−0.1 +/− 0.4	1.2 +/− 0.1	−97.6 +/− 6.88	0.56
C11	−0.14 +/− 0.15	−3.47 +/− 0.41	6.38 +/− 0.57	0.59	4.41 +/− 0.8	−2.4 +/− 0.6	−0.1 +/− 0.2	−97.9 +/− 146.	1.29
C11	−0.15 +/− 0.16	−3.30 +/− 0.43	6.00 +/− 0.59	0.63	4.36 +/− 0.7	−2.2 +/− 0.5	−0.1 +/− 0.2	−172. +/− 113.	1.00
C12	−0.99 +/− 0.15	−4.00 +/− 0.41	7.65 +/− 0.56	0.58	3.12 +/− 0.4	−0.9 +/− 0.3	−0.2 +/− 0.1	−261. +/− 34.0	0.45
C12	−0.98 +/− 0.15	−3.83 +/− 0.42	7.65 +/− 0.58	0.62	2.36 +/− 0.3	−0.6 +/− 0.2	−0.4 +/− 0.1	−243. +/− 13.5	0.28
C13	0.213 +/− 0.13	−3.38 +/− 0.37	5.74 +/− 0.50	0.47	2.19 +/− 0.5	−1.9 +/− 0.4	−0.3 +/− 0.1	−175. +/− 27.8	0.57
C13	0.134 +/− 0.14	−3.26 +/− 0.38	5.83 +/− 0.52	0.50	2.49 +/− 0.5	−1.6 +/− 0.3	−0.4 +/− 0.1	−210. +/− 22.1	0.49
C14									
C14									
E02	0.055 +/− 0.17	2.632 +/− 0.47	−1.2 +/− 0.65	0.78					
E02	0.020 +/− 0.18	2.448 +/− 0.49	−1.1 +/− 0.67	0.84					
E03	0.142 +/− 0.13	−0.82 +/− 0.36	2.22 +/− 0.5	0.45	3.22 +/− 0.8	−5.1 +/− 0.5	0.7 +/− 0.2	−276. +/− 16.7	1.20
E03	0.105 +/− 0.12	−1.05 +/− 0.34	2.71 +/− 0.46	0.39	2.89 +/− 0.7	−5.0 +/− 0.5	0.5 +/− 0.2	−291. +/− 22.7	1.02
E04	0.042 +/− 0.15	−0.51 +/− 0.42	3.31 +/− 0.52	0.31	−0.6 +/− 0.7	−1.8 +/− 0.6	0.5 +/− 0.2	−344. +/− 21.0	0.65
E04	0.113 +/− 0.16	−0.92 +/− 0.44	3.53 +/− 0.55	0.35	−0.9 +/− 0.7	−1.8 +/− 0.6	0.5 +/− 0.2	−354. +/− 22.2	0.64
E05	−0.11 +/− 0.22	−0.86 +/− 0.62	2.34 +/− 0.77	0.69	4.36 +/− 0.8	−4.5 +/− 0.6	1.5 +/− 0.2	−421. +/− 9.72	0.78
E05	−0.19 +/− 0.22	−1.03 +/− 0.61	2.66 +/− 0.76	0.66	4.28 +/− 0.7	−4.5 +/− 0.6	1.6 +/− 0.1	−423. +/− 8.79	0.71
E06	−0.19 +/− 0.23	2.356 +/− 0.63	0.03 +/− 0.79	0.72	1.84 +/− 0.7	−2.8 +/− 0.6	1.2 +/− 0.1	−412. +/− 11.4	0.69
E06	−0.27 +/− 0.24	2.269 +/− 0.66	0.30 +/− 0.82	0.79	2.73 +/− 0.7	−4.1 +/− 0.5	1.8 +/− 0.2	−395. +/− 8.44	1.12
S01	0.000 +/− 0.10	−2.44 +/− 0.27	3.25 +/− 0.38	0.26	9.94 +/− 0.5	−8.4 +/− 0.4	0.4 +/− 0.1	−391. +/− 22.5	0.64
S01	−0.04 +/− 0.11	−2.31 +/− 0.29	3.29 +/− 0.40	0.29	9.90 +/− 0.5	−8.2 +/− 0.4	0.5 +/− 0.1	−403. +/− 15.9	0.61
S02									
S02									
S03	−0.64 +/− 0.13	6.921 +/− 0.37	−5.2 +/− 0.50	0.46	2.98 +/− 0.7	−2.2 +/− 0.5	−1. +/− 0.2	−470. +/− 10.4	1.07
S03	−0.51 +/− 0.14	6.651 +/− 0.39	−5.4 +/− 0.54	0.54	2.78 +/− 0.6	−2.1 +/− 0.4	−1. +/− 0.1	−484. +/− 9.18	0.76
S04					2.85 +/− 1.3	2.38 +/− 0.9	5.6 +/− 0.5	−442. +/− 3.86	2.51
S04					2.55 +/− 1.3	2.71 +/− 0.9	5.8 +/− 0.4	−442. +/− 3.62	2.41
S06	−0.82 +/− 0.24	−2.38 +/− 0.67	2.16 +/− 0.92	1.56	2.66 +/− 0.7	−0.4 +/− 0.5	0.7 +/− 0.2	−391. +/− 16.6	1.01
S06	−0.79 +/− 0.24	−2.34 +/− 0.65	2.26 +/− 0.90	1.48	2.39 +/− 0.6	−0.1 +/− 0.4	0.9 +/− 0.1	−399. +/− 11.6	0.76

```
W01
W01
W02  −0.14 +/− 0.11  −2.56 +/− 0.30  4.50 +/− 0.41   0.31  10.5 +/− 0.8   −6.7 +/− 0.5   1.4 +/− 0.2   −448. +/− 8.43   1.21
W02  −0.21 +/− 0.12  −2.23 +/− 0.33  4.36 +/− 0.45   0.38  10.0 +/− 0.6   −6.3 +/− 0.5   1.7 +/− 0.1   −446. +/− 6.24   0.88
W03  −0.27 +/− 0.11  −0.19 +/− 0.32  2.32 +/− 0.44   0.36  −1.0 +/− 0.6   −1.7 +/− 0.4   −0.4 +/− 0.1  −487. +/− 22.9   0.80
W03  −0.33 +/− 0.11  −0.26 +/− 0.31  2.32 +/− 0.43   0.35  −1.3 +/− 0.5   −1.3 +/− 0.3   −0.3 +/− 0.1  −526. +/− 24.2   0.50
W04  −0.55 +/− 0.11  0.396 +/− 0.30  1.29 +/− 0.41   0.31  1.03 +/− 0.5   −1.2 +/− 0.4   −1.0 +/− 0.1  −475. +/− 8.87   0.57
W04  −0.60 +/− 0.12  0.470 +/− 0.32  1.43 +/− 0.44   0.36  0.60 +/− 0.4   −0.8 +/− 0.3   −0.9 +/− 0.1  −485. +/− 8.41   0.40
W05  −0.26 +/− 0.11  3.620 +/− 0.31  −1.5 +/− 0.42   0.33  3.10 +/− 0.5   −0.0 +/− 0.4   0.5 +/− 0.1   −449. +/− 17.1   0.64
W05  −0.26 +/− 0.13  3.417 +/− 0.34  −1.5 +/− 0.47   0.40  3.30 +/− 0.7   −0.4 +/− 0.5   0.6 +/− 0.2   −437. +/− 17.1   1.02
W06  0.587 +/− 0.19  −2.66 +/− 0.55  4.40 +/− 0.69   0.55  4.91 +/− 0.9   −4.1 +/− 0.7   1.0 +/− 0.2   −472. +/− 13.1   0.98
W06  0.555 +/− 0.19  −2.88 +/− 0.54  4.45 +/− 0.68   0.54  4.94 +/− 0.9   −4.1 +/− 0.7   1.1 +/− 0.2   −465. +/− 12.8   0.98
```

A comparison of the model with the model of Greve et al. (1996) shows that in the former one parameter for the gravitational bending ($\propto sin$(EL)) has been removed. The new model contains the same forms for the encoder offsets and the collimation errors as in Greve et al. (1996). EL offset terms (f, g) in the new model matches the later. However, compared to Greve et al. (1996), the 'cos(AZ).sin(EL)' dependent part of the AZ error in has been removed and an extra term 'c.cos(AZ)' has been introduced in the new model. This indicates that a different physical mechanism could be causing the pointing offsets in EL which is dependent on 'cos(AZ-g)', but does not affect the AZ pointing offset itself. This is possible if the centre of gravity of the antennas do not lie exactly along the AZ axis, and the supporting structure has 2 rigid sides 180° apart while rotated about the AZ axis. Then EL error is $\propto cos$(AZ-g) [dependent on distance from the rigid side], and could explain the results. However, to confirm this independent test by the engineering team is needed.

3.2.3 Applicability of pointing model to data taken at later epochs

To test the applicability of the model to the data taken at later epochs, we observed known calibrators using 'grid-pointing' on 30 Jan 2008 and 9 April 2008. After determining pointing errors using 'pxget' [Note: 'pxget' is going to be superseded by 'genplot' after baseline based pointing error determination is upgraded to use Antenna based Gain solutions (*gngridpntg*) to determine antenna based offsets] which uses the Summary file produced from the , the model derived from the combined 26 and 27 Dec 2007 data was used to fit except for the constant offset terms in AZ and EL which were redetermined. Reduced-χ^2 of the fit with an assumed rms of $1'$, was found to be ~ 1 for almost all the cases (except for a few antennas, for which jumps in pointing errors are observed). This indicates applicability of the model provided the constant offset term in the pointing errors are determined and applied after applying the model to the current antenna positions. We also show a plot of the EL pointing errors measured from Grid-pointing observations on 10 April 2008 (data taken at different AZ and EL for different calibrators) after applying pointing model in Fig. 13. The rms pointing errors are $\sim 1'$ (the case for all working antennas except C14, E02 and S04, for which hardware related pointing problem is suspected), which is $\sim 1.5 - 2$ times smaller than what is obtained by not applying the model. This data set was also used to derive model parameters for some of the antennas for which no model was existing from the previous data.

Note: The final model used currently for correcting the systematic offsets is kept in '/odisk/online1/antoff/gmrt.ante.simp.pntg.model.comb' in the Online machines (known as Bhaskar and Aditya at present).

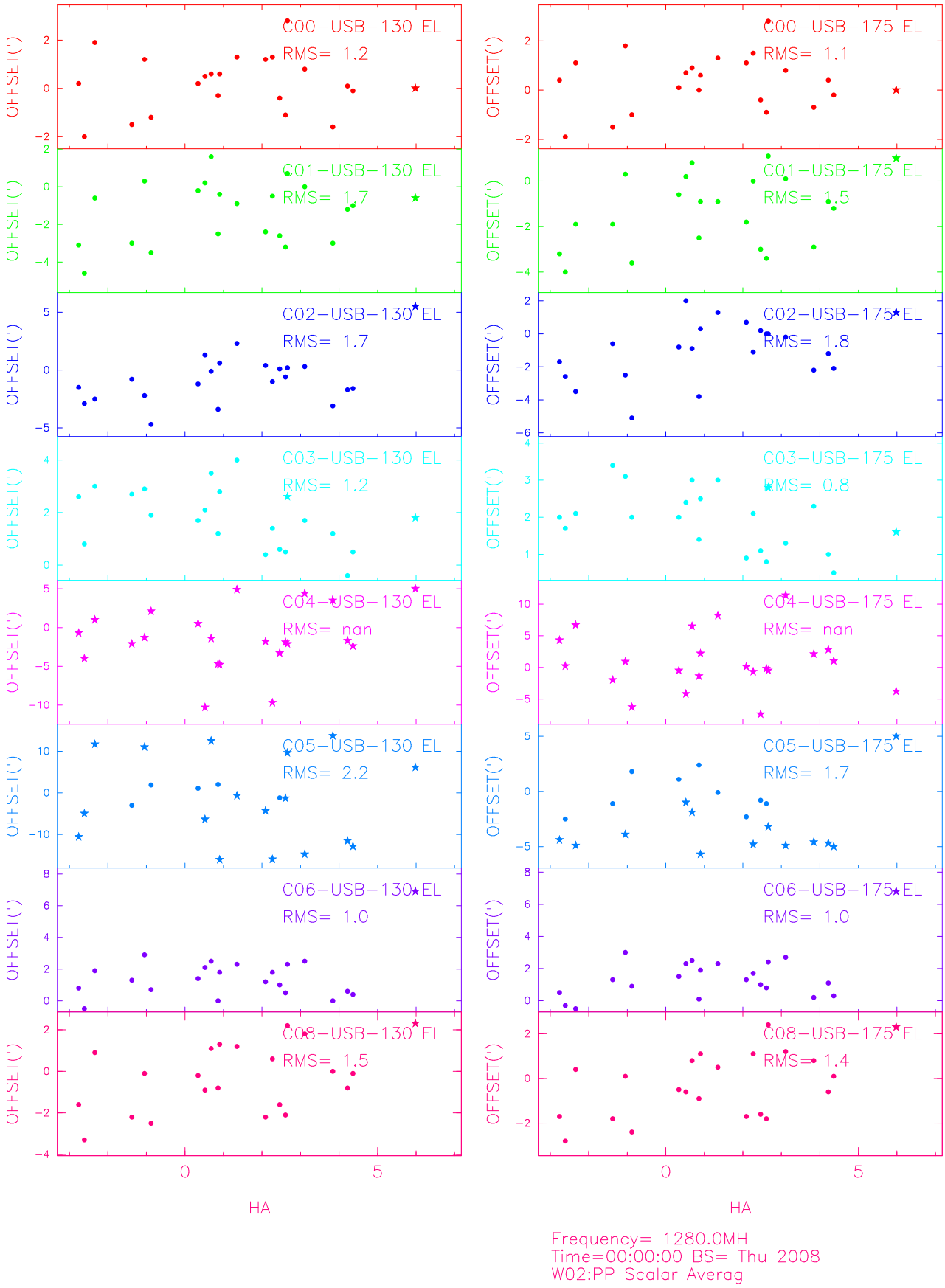

Figure 13. Plot of EL pointing errors as a function of Hour-angle (HA) on 10 Apr 08 after applying Pointing error correction model derived from Dec 07 observations (flagged data points from malfunctioning antennas are indicated by a *).

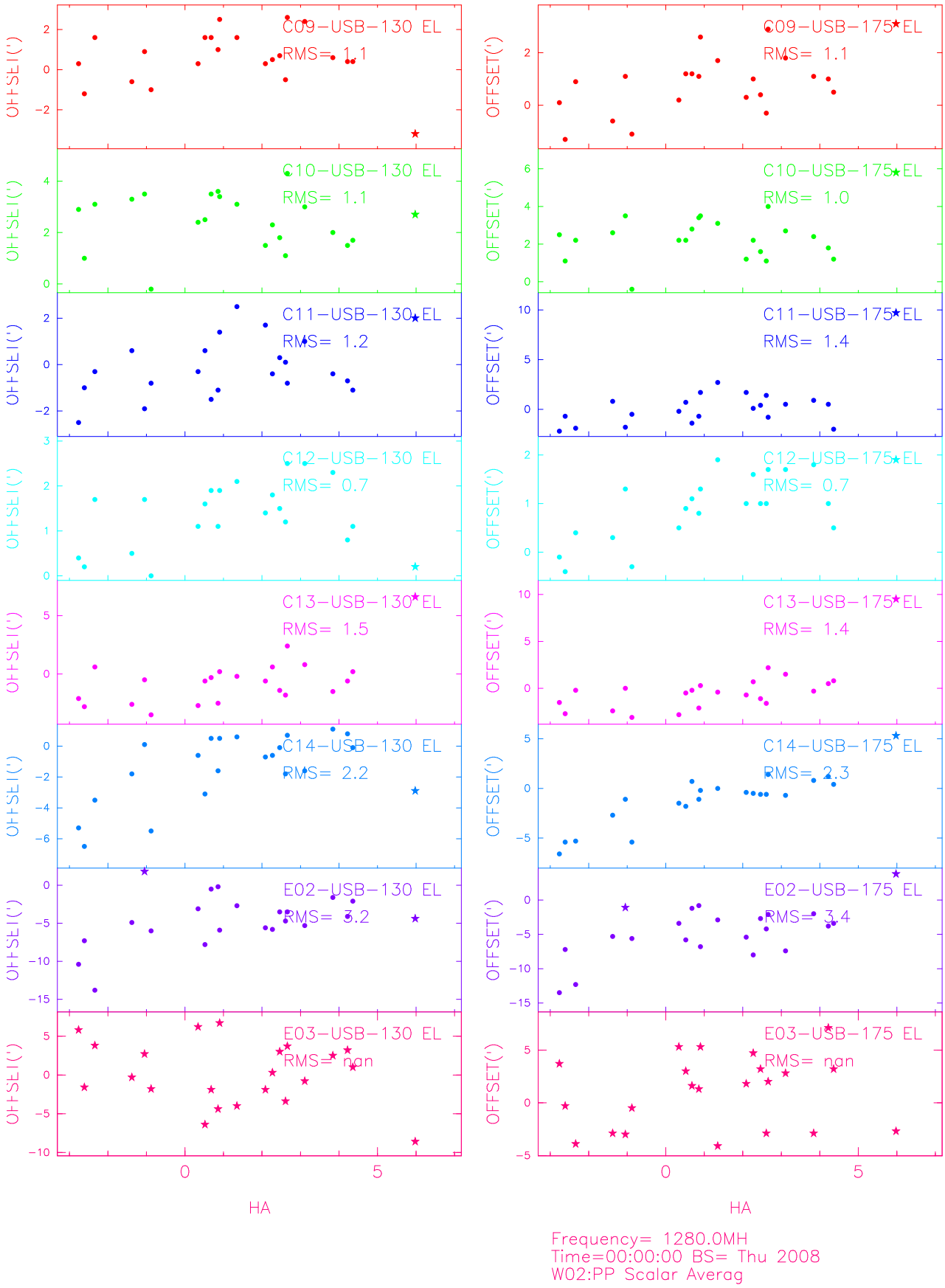

Figure. 13. Plot of EL pointing errors continued...

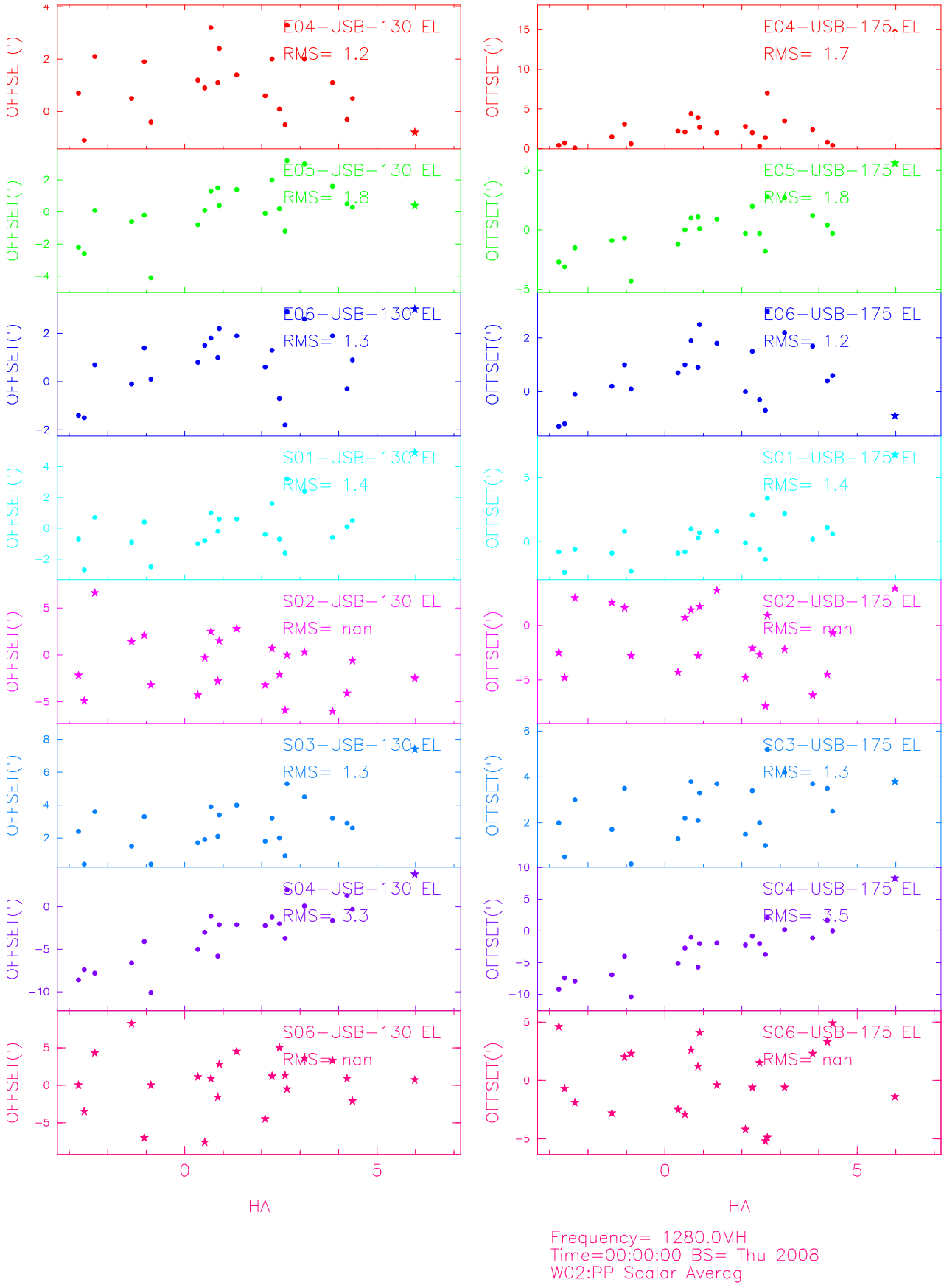

Figure. 13. Plot of EL pointing errors continued...

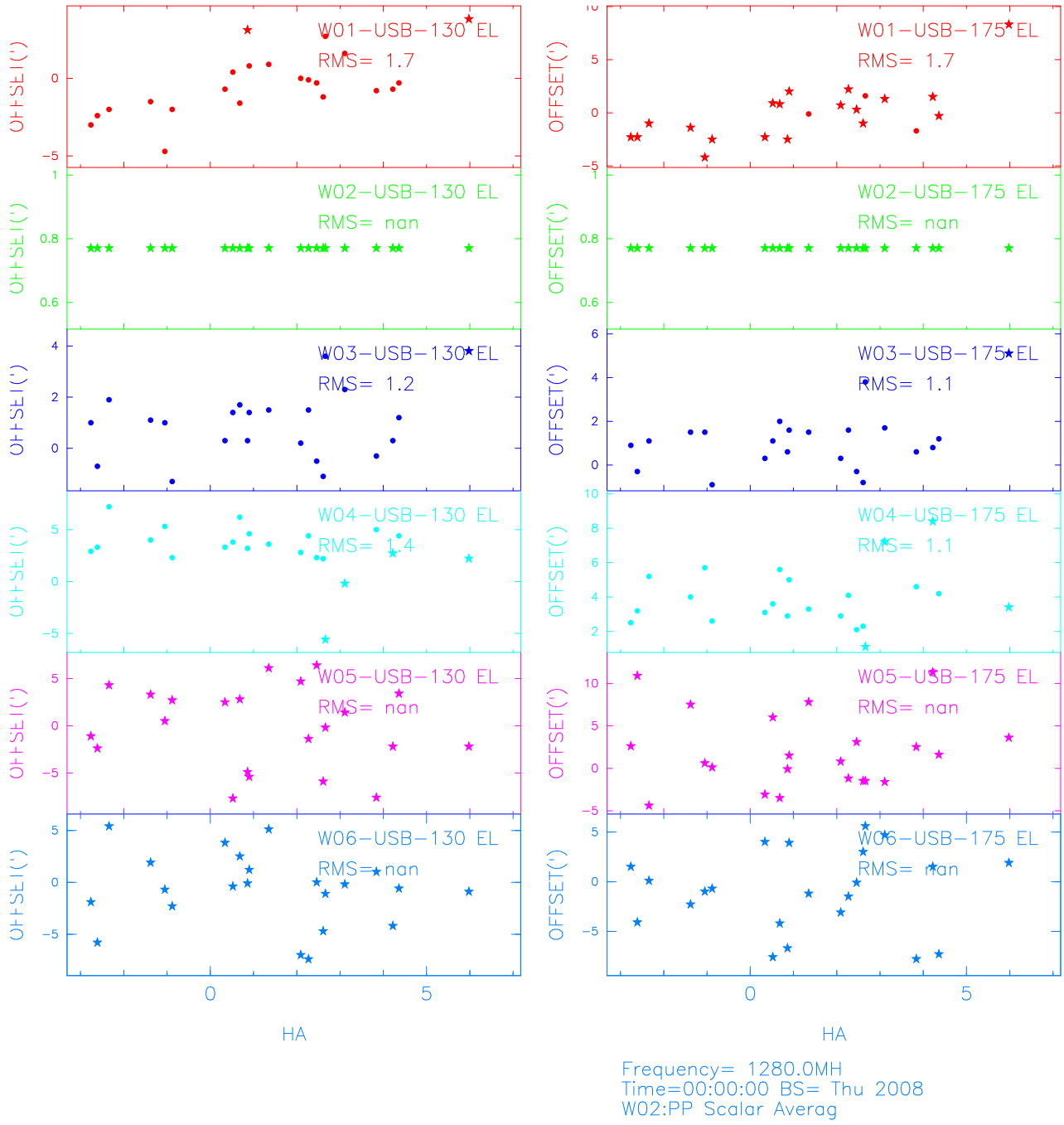

Figure. 13. Plot of EL pointing errors continued...

To check if the above model remains valid even after an year of the data used for obtaining the model parameters, new grid pointing observations were carried out on 21st November 2008 and 29th January 2009. To reduce the need for a continuous long observing time ($\sim$24 hours), we assumed azimuth pointing error is independent of elevation pointing error (found to be accurate from observations done on 12th Jan. 2009 within 1-2$'$ up to ΔEL $<$14$'$ or ΔAZ $<$14$'$ in L band). This allowed to do grid pointing observations only to determine elevation pointing errors for different AZ and EL of the antennas on 21st Nov. 2008 (took $\sim$ 12 hours), and on 29th Jan. similar measurements were carried out for AZ pointing errors at different azimuth and elevation angles towards different calibrators.

We have used the model values in equation (1) and (2) except the constant offsets of the antennas ('a' in Eqn. (1), and 'e' in Eqn. (2)) which changes due to Feed rotation and are fitted to the respective AZ and EL pointing errors data from the above dates with an assumed rms error of 1$'$ (typical servo error). The reduced Chi-square of the fits for all the *working antennas* are shown in Table 4 for the azimuth errors and in Table 5 for the elevation pointing errors data.

Table 4
Reduced Chi-square after fitting the pointing model to the azimuth pointing errors data

Antenna name	Reduced Chisquare	Antenna name	Reduced Chisquare
C00-USB-130	6.74	E05-USB-130	0.53
C00-USB-175	6.55	E05-USB-175	0.59
C01-USB-130	0.17	E06-USB-130	0.26
C01-USB-175	0.28	E06-USB-175	0.32
C02-USB-130	11.0	S01-USB-130	0.26
C02-USB-175	14.3	S01-USB-175	0.22
C03-USB-130	0.64	S02-USB-130	1.09
C03-USB-175	0.87	S02-USB-175	0.70
C04-USB-130	0.24	S03-USB-130	0.12
C04-USB-175	0.55	S03-USB-175	0.08
C05-USB-130	28.1	S04-USB-130	1.12
C05-USB-175	27.9	S04-USB-175	1.31
C06-USB-130	0.56	S06-USB-130	2.68
C06-USB-175	0.60	S06-USB-175	1.97
C08-USB-130	0.19	W01-USB-130	9.62
C08-USB-175	0.26	W01-USB-175	14.7
C09-USB-130	0.88	W02-USB-130	0.11
C09-USB-175	1.22	W02-USB-175	0.23
C10-USB-130	0.32	W03-USB-130	0.40
C10-USB-175	0.38	W03-USB-175	0.17
C12-USB-130	0.25	W04-USB-130	8.09
C12-USB-175	0.44	W04-USB-175	6.30
C13-USB-130	0.11	W05-USB-130	0.15
C13-USB-175	0.15	W05-USB-175	0.16
C14-USB-130	0.87	W06-USB-130	0.39
C14-USB-175	0.41	W06-USB-175	0.49
E02-USB-130	0.40		
E02-USB-175	0.35		
E03-USB-130	0.36		
E03-USB-175	0.46		
E04-USB-130	0.36		
E04-USB-175	0.35		

Table 5
Reduced Chi-square after fitting the pointing model to the elevation pointing errors data

Antenna name	Reduced Chisquare	Antenna name	Reduced Chisquare
C00-USB-130	0.79	E05-USB-130	2.61
C00-USB-175	0.55	E05-USB-175	2.73
C01-USB-130	0.69	E06-USB-130	0.49
C01-USB-175	0.80	E06-USB-175	0.66
C02-USB-130	2.09	S01-USB-130	1.41
C02-USB-175	1.95	S01-USB-175	1.24
C03-USB-130	0.29	S02-USB-130	1.73
C03-USB-175	0.19	S02-USB-175	1.37
C06-USB-130	1.06	S03-USB-130	0.62
C06-USB-175	1.47	S03-USB-175	0.59
C08-USB-130	0.96	S04-USB-130	6.56
C08-USB-175	0.88	S04-USB-175	7.18
C09-USB-130	0.52	S06-USB-130	1.25
C09-USB-175	0.65	S06-USB-175	0.90
C10-USB-175	0.66	W01-USB-130	0.60
C12-USB-130	0.13	W01-USB-175	0.48
C12-USB-175	0.10	W02-USB-130	0.83
C13-USB-130	0.70	W02-USB-175	1.33
C13-USB-175	0.71	W04-USB-130	6.65
C14-USB-130	1.19	W04-USB-175	4.68
C14-USB-175	1.62	W05-USB-130	0.45
E02-USB-130	5.45	W05-USB-175	0.35
E02-USB-175	5.25	W06-USB-130	0.31
E03-USB-130	0.99	W06-USB-175	0.28
E03-USB-175	1.54		
E04-USB-130	1.69		
E04-USB-175	1.60		

As can be seen from the values of the reduced Chi-squares of the fits that except for a few antennas, the fits to the data are good (Reduced Chi-square ~ 1). Plots of the data (Red Colour points ('+' sign)) and the residuals (Green colour points ('x' sign)) after model fitting to the data are shown below in Figures 14 and 15.

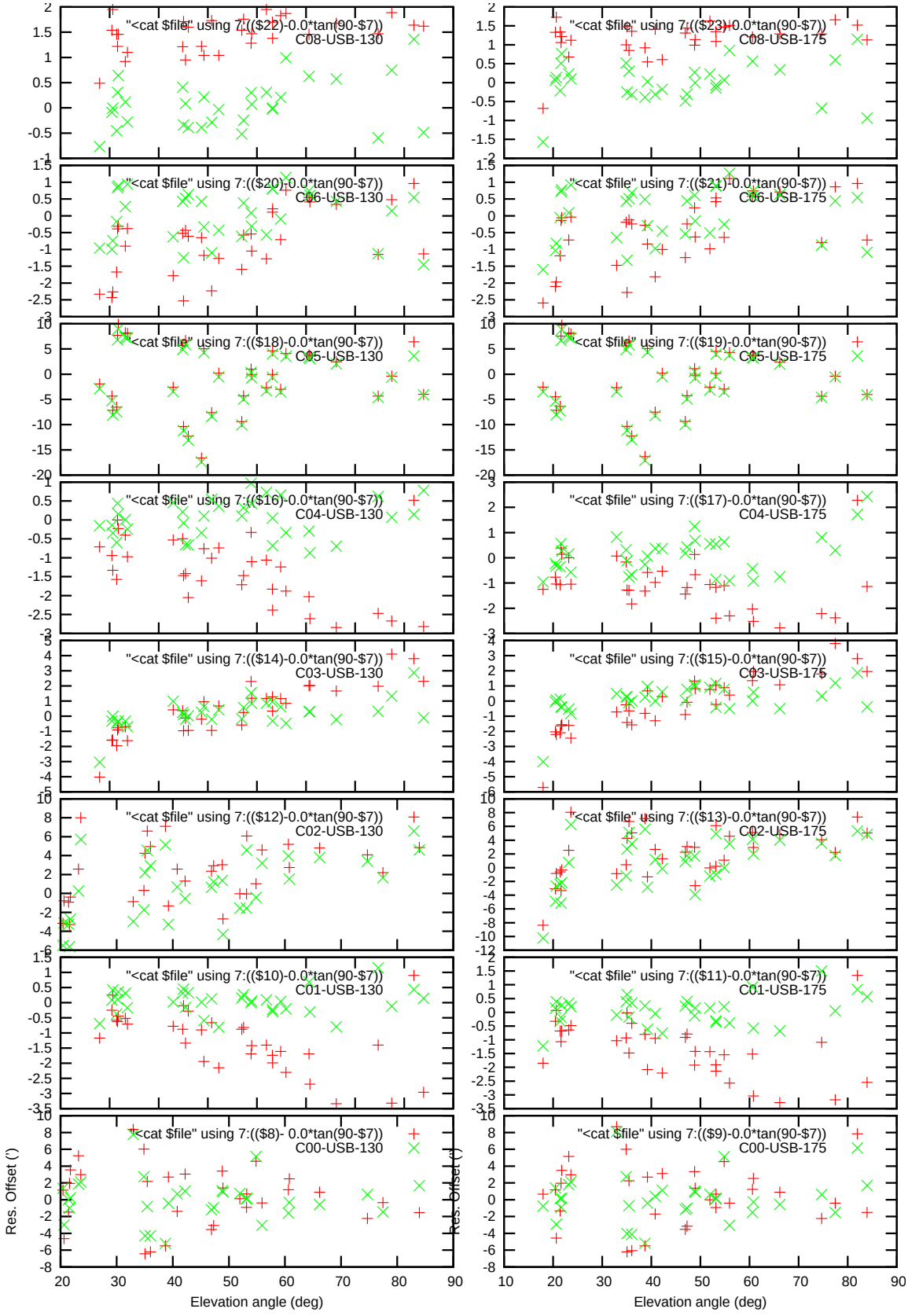

Figure 14. Plot of AZ pointing errors (in arc-min) as a function of elevation angle (EL) on 29th Jan. 2009. The Red colour points ('+' sign) show the actual offsets measured, while the Green colour points ('x' sign) indicate the same points after subtracting the fitted pointing model (see text).

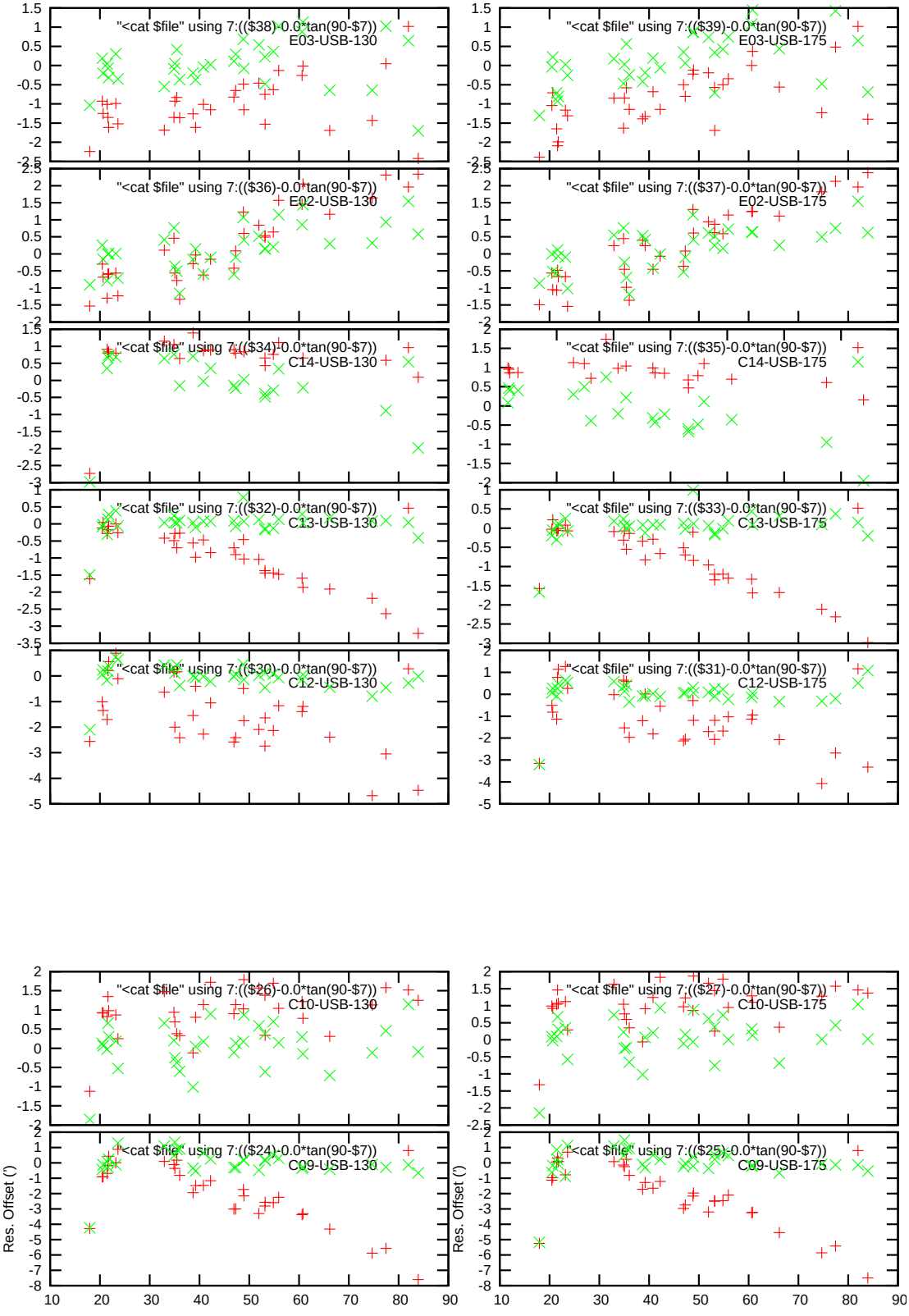

Figure 14: Plot of AZ pointing errors continued ...

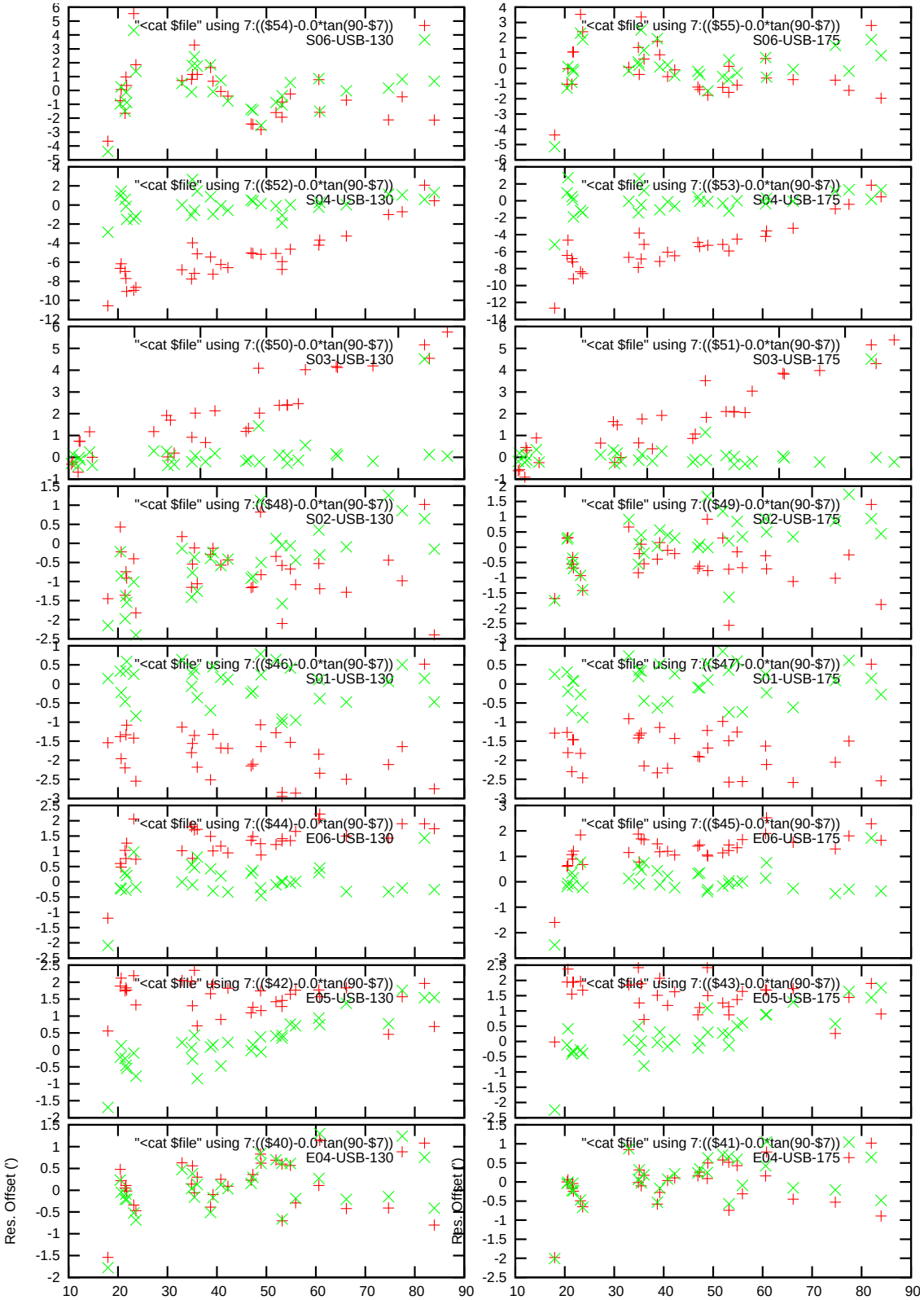

Figure 14: Plot of AZ pointing errors continued ...

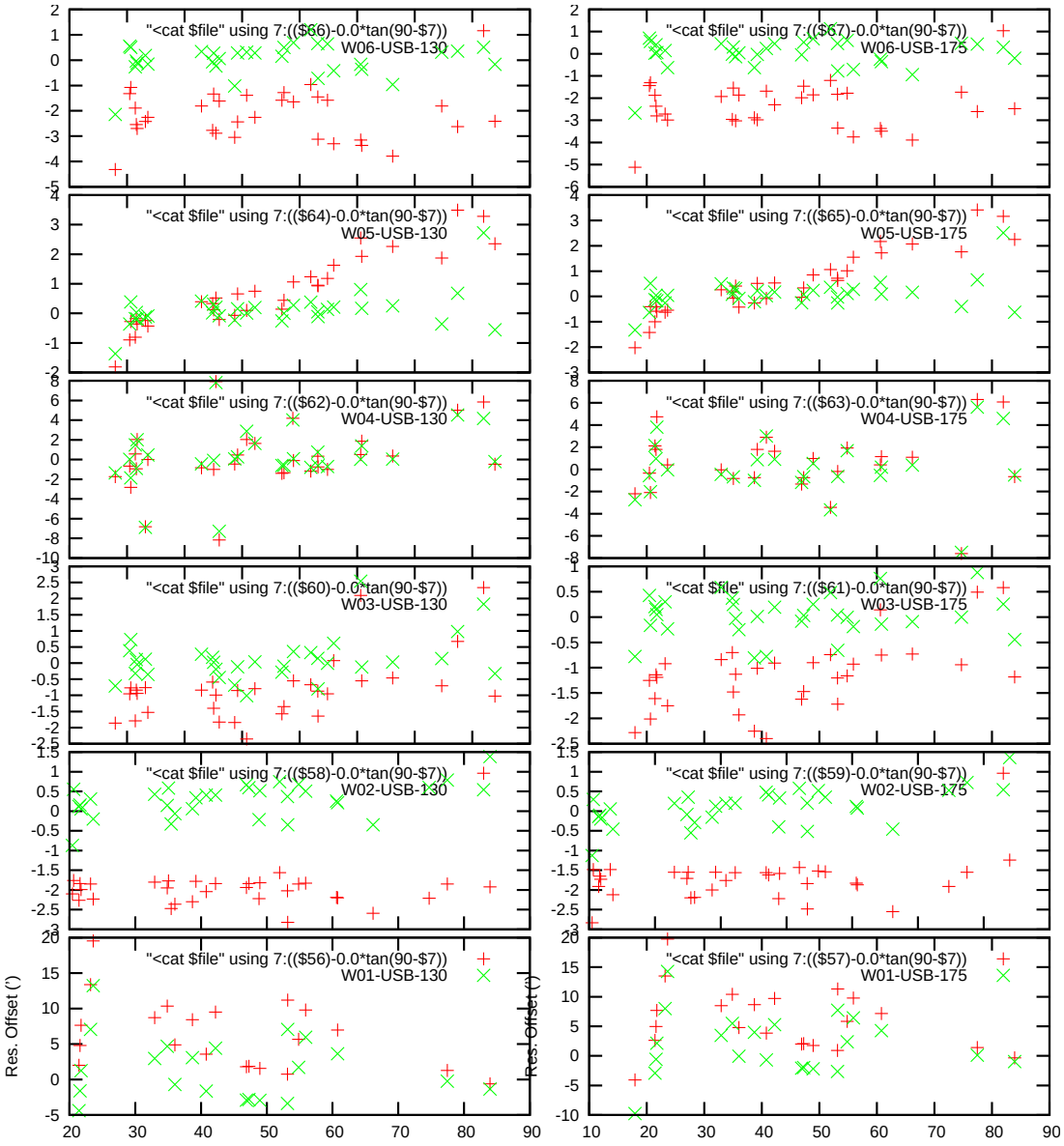

Figure 14: Plot of AZ pointing errors continued ...

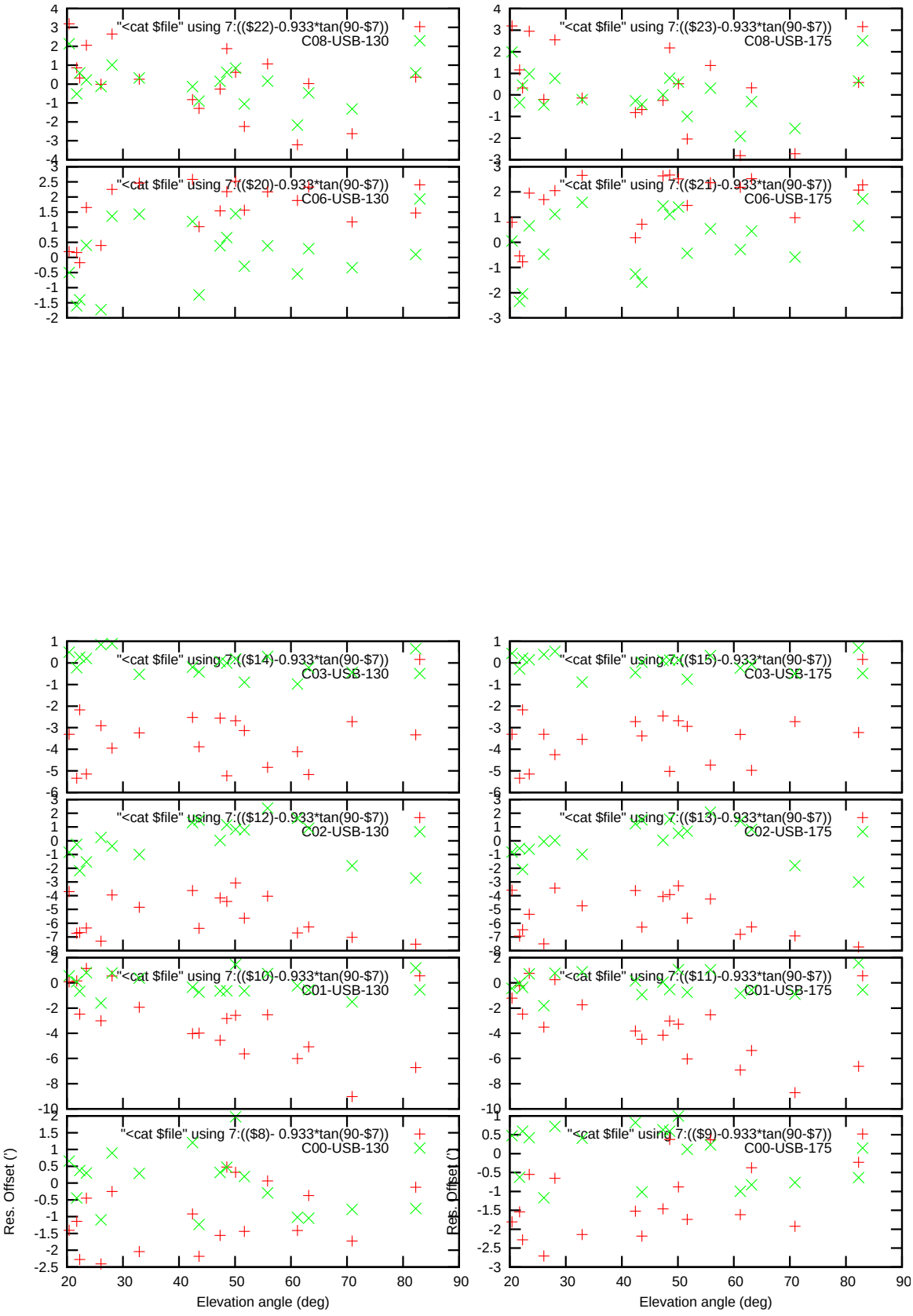

Figure 15. Plot of EL pointing errors (in arc-min) as a function of elevation angle (EL) on 21 Nov 08. The Red colour points ('+' sign) shows the actual offsets measured, while the Green colour points ('x' sign) indicate the same points after subtracting the fitted pointing model (see text).

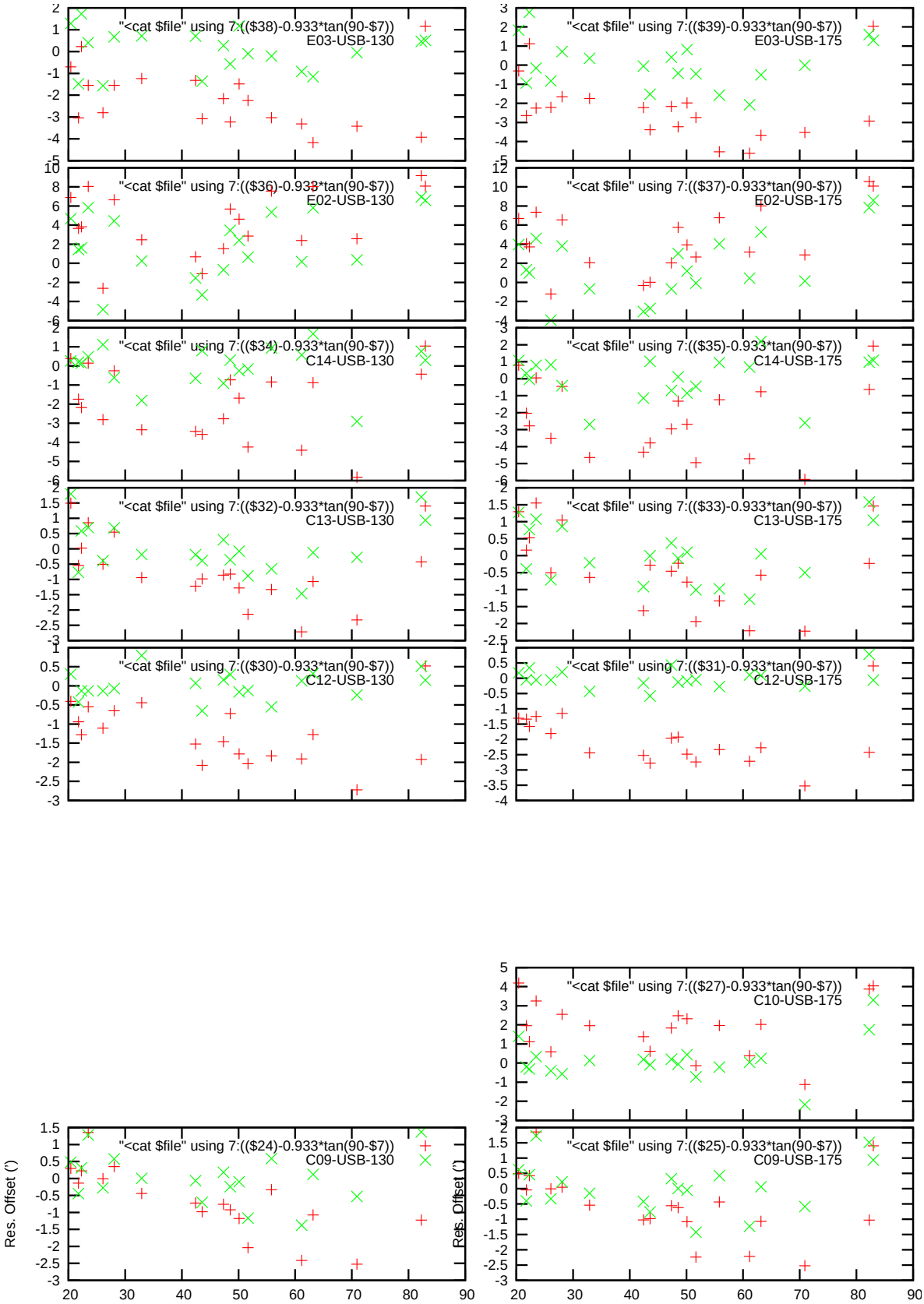

Figure 15: Plot of EL pointing errors continued ...

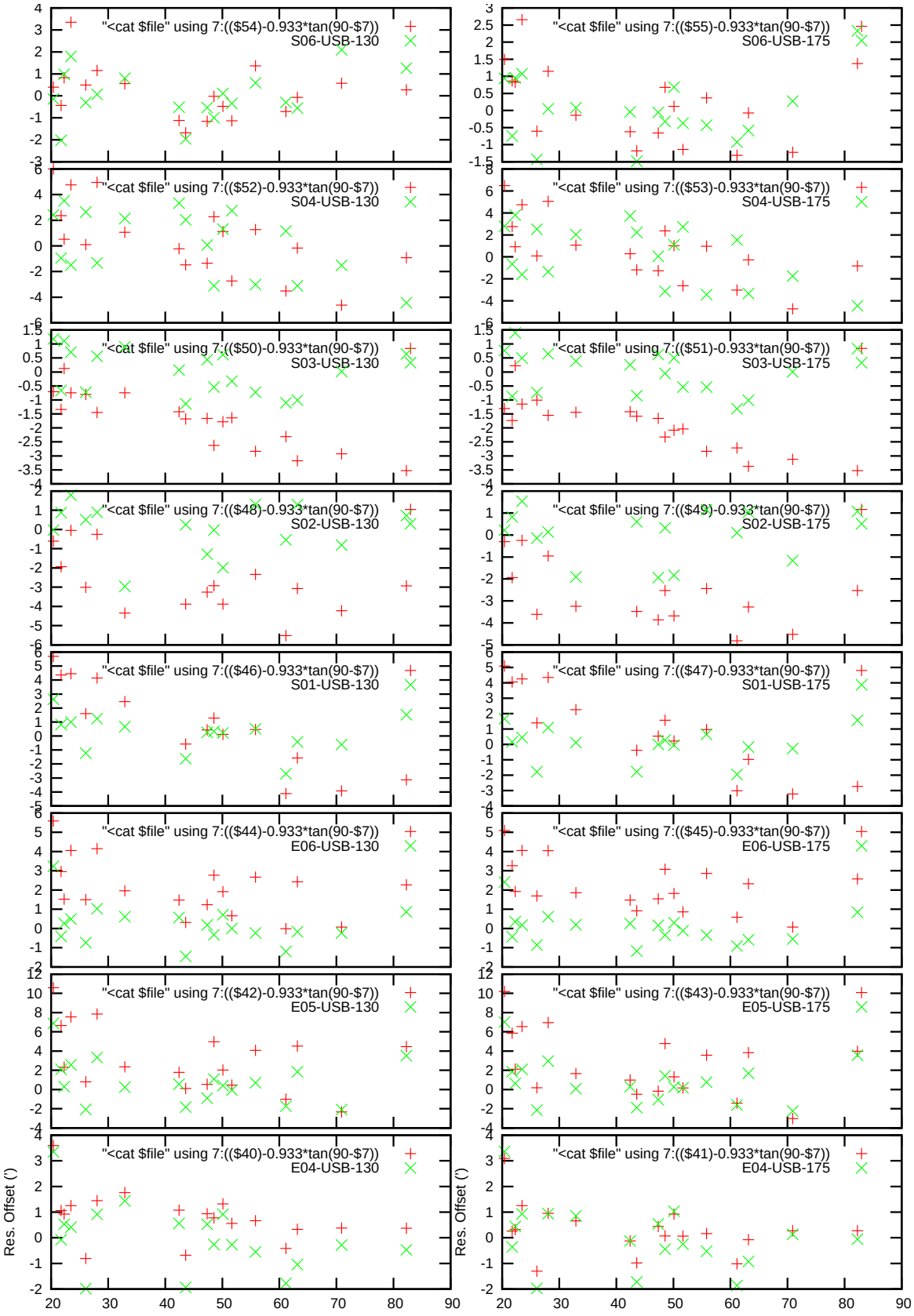

Figure 15: Plot of EL pointing errors continued ...

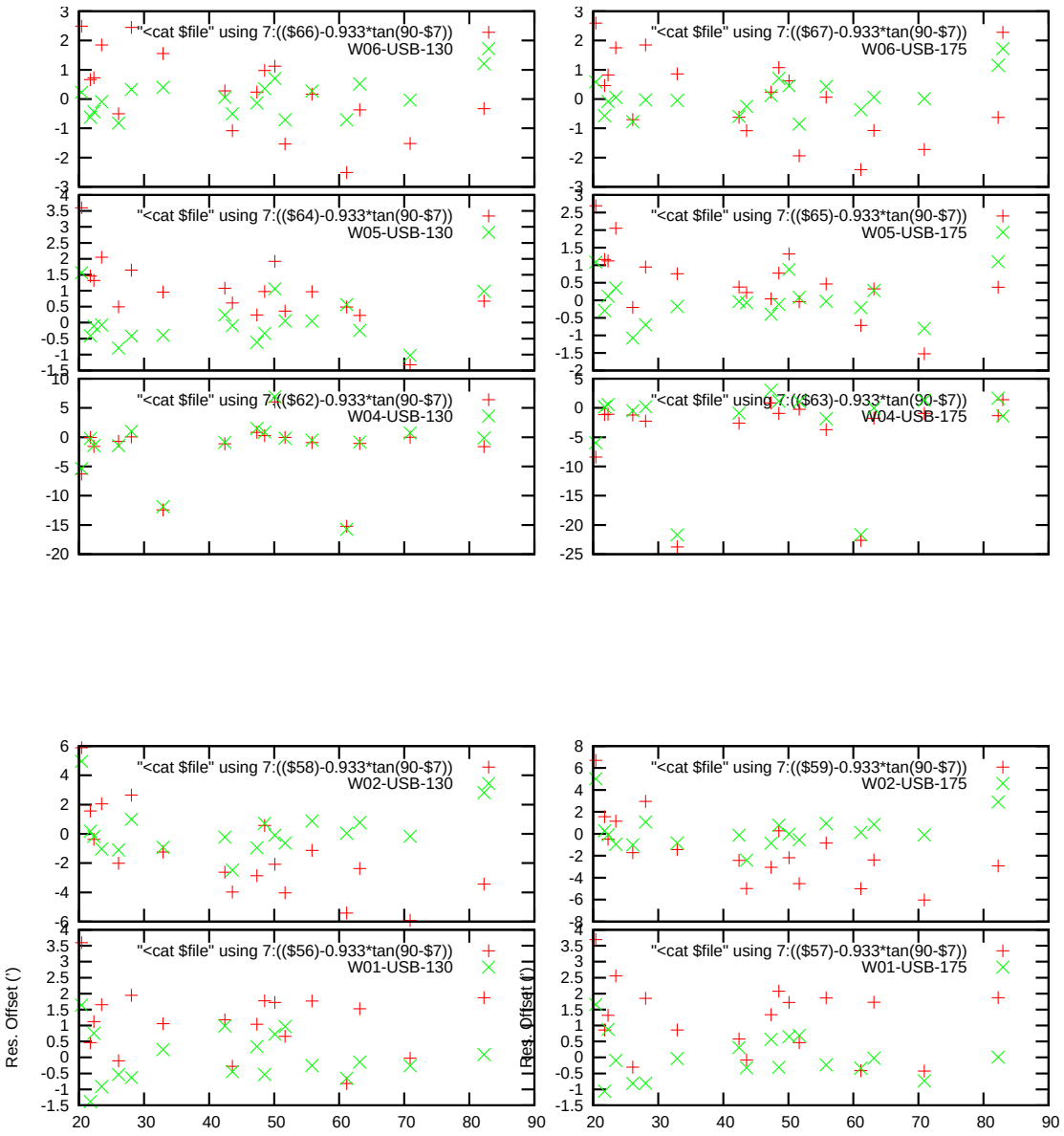

Figure 15: Plot of EL pointing errors continued ...

As can be seen from reduced Chi-square values (Table 4 & 5) and the plots, other than C00, C02, C05, W01 and W04 in azimuth and E02, S04 and W04 in elevation, pointing errors for the rest of the antennas can be well fitted with the existing model.

Notes on antennas having large residual pointing errors near the end of the year 2008:

Among the antennas affected, C05 has been found to have large errors in AZ pointing for the last one year. C00 and W01 had lack of accuracy in AZ pointing 6 months back, and have worsened at present. C00 and C05 appear to show sudden change in pointing errors (*jumps*) in AZ axis around AZ=50°, while C02 shows *jump* around AZ $\sim$ 0°. W01 and W04 do not appear to show any clear jump, but may be highly erratic (need to be monitored). However, S04 in AZ did not show any jump (was bad for many months) and appear to have worked fine.

During EL grid pointings, E02 has consistently shown *jumps* up to $\sim 10'$ for hour angles $<$2 hour in the last one year. S04 also showed large residuals. Given that EL pointing was done 2 months before AZ pointing, it could indicate that S04 pointing problems have gone away in the meantime.

4 Online application of the model

3 different Python scripts written: (i) to generate Command file for grid pointing with user supplied reference antennas and grid spacings (gridpntg_cmd_create.py), (ii) to generate new Pointing Offsets file given the previous Offset file incorporating corrections determined from Grid-pointing (gridpntg_update.py) and (iii) to Generating new Offset file for antennas given the Default Offset file and the pointing model (pntg_model_apply.py).

4.1 Details of the scripts and Online usage:

1. 'gridpntg_cmd_create.py' was written to generate the Command file used for measuring Pointing error on a calibrator, which requires using a reference antenna. The Online needs to use 2 different sub-arrays, where one sub-array contains the reference antenna(s) tracking the source with no offsets, and the other one contains antennas which are tracking the source with known variable angular offsets from the source [this is going to change with using just 'one' subarray when the antenna based gain solutions (rantsol) are used to find Pointing offsets using a programme called *gngridpntg*]. Since defining sub-arrays require using antennas by their numbers, this script converts the reference antenna name to its number known to the Online, and write the Command file using valid syntax. The generated file can be edited for more fine-tuning. The script can take up to six command line parameters. These are (i) source_name, (ii) Obs_band (MHz), (iii) track (outer/inner track for the antennas), (iv) No_of_grids (defaults to 9, if no corresponding entry is specified on the command line). This is used to specify the number of grid points used for pointing error measurements. Note that the maximum angular distance the antennas move from the source at a particular frequency is taken to be constant. Therefore, more number of grid points do not increase the maximum angular distance the antennas move from the source, but only reduces the angular separation of the grid-points. The maximum angular distance the antennas move from the source at 1420 MHz is $28'$. This maximum angular separation is a combination of 2 terms. The first part is directly proportional to the wavelength of observation, and is taken to be $12'$ at 1420 MHz. The second part is independent of wavelength, which is $16'$ used to account for antennas having comparatively large pointing errors at the start of observation. (v) Command_file. This provides the name of the Command file generated. Defaults to '/odisk/gtac/cmd/pntg/gpntg.cmd', if nothing is specified on the command line. (vi) EL_or_AZ (needs to be specified **only if** the command file is meant for generating one of EL or AZ scan). Note that the input parameters while generating the Command file are appended to the '/odisk/online1/antoff/pointing.offsets.cumulative' file (mounted on the Online machines). Running the generated Command file for Grid-pointing observations takes about 30 minutes.

'gridpntg' (written by Vasant Kulkarni using Perl) is used to determine the Pointing offsets from the 'lta' file produced by running the Command file mentioned above. This programme requires a input parameter file containing (i) the name of the 'lta' file; (ii) Reference antenna (e.g.: W02) ; number of frequency channels to use during the fit in the format: Start Channel, last channel, increment (e.g.: 20,100,1); pointing mode for which solution is sought (either A for Azimuth, or E for Elevation); and the Grid parameters used during the Grid-pointing in the format: Starting offset, end offset , increment (e.g.: -28,28,7).
Each of the above parameters need to start in a separate line of the parameter file.
Note: 'gridpntg' is going to be superseded by *gngridpntg*, which is based on antenna based gains, and as such will need the Reference antenna only to keep the Phase Zero for that antenna while determining the gains.
The output text files contain the measured Offsets for the antennas.

2. 'gridpntg_update.py' is used to update the file (/odisk/online1/antoff/NLDANTO.001) which is used to correct the pointing errors of the antennas. It can take up to 3 command line parameters. (i) Pntg_Error_file_az. This file provides the AZ pointing errors measured from the above Grid-pointing observations. The first 10 lines of this file are treated as headers and skipped. The entries in the 'Pntg_Error_file_az' need to have antennas ordered Row wise with each antennas having 2 measurements corresponding to 2 different polarisations. The 1st column denotes the antenna name, the 2nd a string corresponding to the type of observation (AZ), the 3rd denotes the measured pointing offsets and the 4th one denotes the weights for each of the measured offsets, with higher weights denoting more accuracy and reliability. All the pointing offsets $\geqslant 2'$ with weight of 2 or more are used to update the corresponding entries in the file (/odisk/online1/antoff/NLDANTO.001) used for correcting the pointing errors of the antennas. (ii) Pntg_Error_file_el, which provides the EL pointing errors measured from a Grid-pointing observations. It has the same format as the file in (i). (iii) Offset_file, which defaults to '/odisk/online1/antoff/NLDANTO.001', if no corresponding file-name is provided on the command line.
The format of the default pointing error file (NLDANTO.001) need to be such that the names of each antenna appear serially along the rows of the file. Each column of that file containing the antenna names provide the Pointing offset in a format 'ANTENNA_OFF(AZ′, EL′)'.
Note that while generating the new pointing offset file (/odisk/online1/antoff/NLDANTO.001), for documentation, the earlier entries in that file gets appended to another file '/odisk/online1/antoff/pointing.offsets.cumulative' before being overwritten by the new entries. Hence, the last entry for the antennas could be used to regenerate the default pointing offset file (/odisk/online1/antoff/NLDANTO.001) in case the offsets in that file is suspected to be faulty due to any problem (should not be required in general).
Reasonable precautions are taken so that typing error in the name of 'Pntg_Error_file_az' or 'Pntg_Error_file_el' could be detected (programme aborts) and multiple use of the same 'Pntg_Error_file_az' or 'Pntg_Error_file_el' cannot be made.
It is possible to update the pointing offset file, when only one of AZ or EL errors are measured. The option inside the script do not work at present, and one needs to use a dummy file for the missing measurement (e.g., when AZ measurements are not available, use 'Pntg_Error_file_az' having '0' as the AZ pointing error).

3. 'pntg_model_apply.py' is used to apply a known pointing error model (derived from pointing error measurements including refraction due to neutral atmosphere) to the current position (AZ, EL) of the antennas and predict the correct pointing directions of the antennas so that there is no resultant pointing errors during observations. It can take up to 2 options, (i) Offset_file. The name of the file of known constant offsets for the antennas (/odisk/online1/antoff/NLDANTO.001). (ii) 'Model_file', defaults to '/odisk/online1/antoff/gmrt.ante.simp.pntg.model.comb', if no corresponding name of a file is provided on the command line. The script uses a programme 'azel.new' which queries the Online for the current location of the antennas and uses that AZ and EL in the model for the antennas and estimate a pointing errors for them. The modified pointing offsets are written to a unique file named according to '/odisk/online1/gridpntg/NLDANTO-DD,MM,YYYY,:HH,MM,SS,'. This file is then *linked* to '/odisk/online1/gridpntg/PMANTO.001', which is actually used by the Online to correct for the present pointing errors of the antennas.
The script also write another file '/home/operator/runfil/OFFSET.DAT', which is used by the Online to compute the difference between the target and the actual pointing directions of the antennas ('sacw').
The 'Model_file' has a format where all the 30 antennas need to appear serially rowwise. The antenna name and the 7 parameters ('a' to 'g') used to describe the pointing model appear column wise respectively.

4.1.1 Online usage during observations:

Application of the pointing error model during observations is done in 2 steps. (i) a shell script '/home/odsoft/bin/pntmod' is called (typing '/pntmod' from the Online Aips shell), which simply calls 'pntg_model_apply.py' with '/odisk/online1/antoff/NLDANTO.001' as the first argument. (ii) The modified pointing offset file is then used to correct the pointing errors of the antennas by loading it from Online Aips shell (typing 'run PMANTO' from the Online Aips shell). The above 2 lines are also used in the user Command file to correct for the antenna based pointing errors. It is suggested that the users put the above 2 lines in their Command file for all observing frequencies above 330 MHz. The model could be applied every half an hour to once in an hour. Since many users observe a calibrator once in about half an hour, they could put the above 2 lines after the 'sndsacsrc' command is used to move the antennas towards the Target source after observing a calibrator. Note that updating the pointing offsets takes about 2 minutes of time at present with the Online machines.computers.

5 Conclusion

In this work we have shown that it is possible to properly model the AZ and EL dependent pointing errors observed with the GMRT antennas including refraction correction for the neutral atmosphere. A 7 parameter (3 parameters for AZ and 4 parameters for EL pointing errors) model could fit the AZ and EL pointing data reliably. The parameters of the model appear to remain stable (except the constant offsets terms) over a timescale of an year, and using it could reduce typical pointing errors by ~ 2. The model is now applied Online on regular basis, and in this report we have also provided details of its implementation. However, there are ~ 5 antennas, which seem to have unexplained behaviours, which could be related to hardware problems. For these antennas, model parameters could not be derived reliably. It is possible that the model parameters could change on timescales of $\gtrsim 1$ year. Therefore, the pointing model need to be checked periodically for its validity.

Acknowledgements

We thank Jitendra Kodilkar, who mostly wrote the Online 'grid-pointing' routine for using it during regular Grid-pointing observations. We also thank A. Pramesh Rao for his suggestions on modifying the Online system for incorporating changes in the Grid-pointing routine to make it run without user's presence most of the time. Deepak B Bhong wrote the programme 'azel' which provides the target location of the antennas from the Online and we thank him for doing that. Nimisha G. Kantharia was involved in the determination of the earlier pointing model parameters and we thank her for insightful discussions on the topic. We also acknowledge various discussions on the topic with Yashwant Gupta.